RSC Sustainability

ROYAL SOCIETY OF CHEMISTRY

CRITICAL REVIEW

View Article Online
View Journal | View Issue

Cite this: *RSC Sustainability*, 2025, **3**, 4314

Advances in lead-free perovskite solar cell design *via* SCAPS-1D simulations

Vívian Helene Diniz Araújo, *[a] Ana Flávia Nogueira, [b] Juliana Cristina Tristão [a] and Leandro José dos Santos [a]

Perovskite solar cells (PSCs) have attracted significant attention over the past decade due to their high performance. However, challenges such as moisture sensitivity and the toxicity of certain constituents remain barriers to their commercialization. Tin, germanium, and other elements with optoelectronic properties similar to those of lead have emerged as promising substitutes for the B-site metal in PSCs. Theoretical studies have played a crucial role in elucidating how specific material and structural parameters influence photovoltaic behavior. Among the most prominent tools for simulating thin-film solar cells in recent years, open-source SCAPS-1D software stands out as a valuable resource. Therefore, this article presents a comprehensive review of 54 simulation studies, using SCAPS-1D, published between 2016 and 2025, focusing on lead-free PSCs. In total, 26 studies on Sn-based PSCs and 28 on perovskites with alternative B-site metals were analyzed to evaluate how simulations have contributed to understanding device performance with lead substitutes. This review also provides an overview of the current research landscape and highlights promising directions for advancing environmentally benign, lead-free PSCs through SCAPS modeling. The studies discussed in this review show a prevailing tendency to simulate PSCs in regular rather than inverted configuration. In many cases, the defect density assumed for the absorber layer is set at ideal values or even below 10^{13} cm^{-3}, which potentially limits the accuracy of predictions. Among the strategies adopted to improve performance, composition engineering emerged as the most prominent.

Received 29th June 2025
Accepted 21st August 2025

DOI: 10.1039/d5su00526d

rsc.li/rscsus

[a]*Universidade Federal de Viçosa – Campus Florestal, UFV, Rodovia LMG 818, km 06, s/n, Campus Universitário, Florestal, MG, Brazil. E-mail: vivian.helene@ufv.br*

[b]*Universidade Estadual de Campinas, UNICAMP, Cidade Universitaria Zeferino Vaz, Campinas, SP, Brazil*

Vívian Helene Diniz Araújo

PhD student in Chemistry at the Multicentric Graduate Program in Chemistry (PPGQM-MG) through the Federal University of Viçosa, with a focus on organic synthesis, working at the QuiTam Research Laboratory (Laboratory of Chemistry and Environmental Technologies). Experienced in the synthesis of novel fulleropyrrolidines and solar cell simulations. Took maternity leave for six months in 2021. Holds a Master's degree in Chemistry (2020) from PPGQM-MG (UFV), where she worked at the Laboratory of Analysis and Synthesis of Agrochemicals (LASA), synthesizing esters for potential agrochemical applications. Licentiate degree in Chemistry from the Federal University of Viçosa – Florestal Campus (2017). Currently, Vívian works as a full-time high school Chemistry teacher in the state of Minas Gerais, Brazil.

Ana Flávia Nogueira

Prof. Ana Flávia obtained her bachelor's degree in Chemistry from the University of São Paulo (1996) and Master (1998) and PhD degrees in Chemistry from the University of Campinas (2001). She worked as a post-doctorate fellow at the Imperial College, UK, from 2001–2002 and as visiting researcher at Stanford University from 2017–2018. At the moment, Ana Flávia is a Full Professor at the Chemistry Institute at UNICAMP and Director of the Center for Innovation on New Energies. Prof. Nogueira's research focuses on the development of functional (nano)materials and their application in solar energy conversion. She has experience in the field of perovskite solar cells, perovskite quantum materials and dense energy carriers (generation of solar fuels through photoelectrocatalytic systems using water, CO_2 and other low-added values substrates).

Sustainability spotlight

Perovskite solar cells (PSCs), although considered a promising photovoltaic technology, still face challenges for commercialization, particularly the use of toxic metals such as lead. The replacement of lead by alternative metals like tin, manganese, and bismuth has been widely investigated by the scientific community. The Solar Cell Capacitance Simulator in One Dimension (SCAPS-1D) is a free software tool commonly used to model lead-free thin-film solar cells. Our critical review analyzed 54 simulation studies, identifying both promising trends and methodological inconsistencies that often lead to unrealistic efficiency predictions. This work is aligned with SDG 7 (Affordable and Clean Energy) and SDG 11 (Sustainable Cities and Communities).

1 Introduction

Considered an emerging photovoltaic technology with great potential, perovskite-based solar cells (PSCs) serve as efficient light absorbing materials, demonstrating high energy conversion rates, exceeding 20%, and lower production costs compared to their silicon-based counterparts.[1] Planar PSCs can be configured in both regular (n–i–p) or inverted (p–i–n) architectures, depending on whether the incoming light first reaches the electron transport layer (ETL) or the hole transport layer (HTL), as illustrated in Fig. 1.

Numerous experimental and theoretical studies have been conducted to address the challenges that hinder the reproducibility and commercialization of PSCs. One of the main barriers to commercialization is the presence of environmentally toxic elements in their composition, particularly lead.[2,3]

Tin is the leading candidate to replace lead in PSCs due to their similar structural characteristics, since both elements belong to the same group (IVA) in the periodic table. Tin-based perovskites, such as $CH_3NH_3SnI_3$ (MASI), which uses methylammonium as the organic cation, and $CH(NH_2)_2SnI_3$ (FASI), which incorporates formamidinium at the A site, are among the most commonly used in experimental studies on lead-free PSCs.[4,5] Other metals, such as germanium and bismuth, are also being studied as alternative solutions for the development of lead-free PSCs.

Table 1 summarizes the main experimental works conducted on Pb-free PSCs, all using tin perovskites, which still exhibit the best performance among the metals used as lead substitutes.

In recent years, numerous simulation studies have focused specifically on lead-free PSCs,[12–15] aiming to understand how to improve the efficiency of these devices. Computational simulations of solar cells enable a deeper investigation into the influence of various parameters on device performance. By adjusting the properties of individual layers and their interfaces, these simulations allow researchers to assess the impact of defects, ultimately saving time and resources during experimental development.[16,17]

SCAPS-1D (Solar Cell Capacitance Simulator in One Dimension) is a widely used software for simulating a variety of thin-film solar cell structures. Developed in 1996 by the research team led by Niemegeers and Burgelman,[18] the program is based on the fundamental equations of semiconductor physics: the Poisson equation, the continuity equations for electrons and holes, and the current equations (drift-diffusion). The software is particularly suitable for modeling polycrystalline

Juliana Cristina Tristão

Ph.D. in Inorganic Chemistry (2010), a Master's degree in Inorganic Chemistry (2007), and a Bachelor's degree in Chemistry from the Federal University of Minas Gerais (2005). She completed a research internship at the Department of Chemistry, University of Montreal (Canada, 2005), focusing on nanotube synthesis. Currently, Prof. Juliana is an Associate Professor at the Federal University of Viçosa, where she primarily teaches courses in Analytical Chemistry. Her research has focused on nanotechnology applied to processes of environmental and technological relevance, including carbon nanotubes, iron oxide-based magnetic nanoparticles, adsorption processes, heterogeneous Fenton reactions, heterogeneous catalysis involving nanoparticles, biodiesel synthesis, and the reutilization of bio-oil and biomass. She coordinates the QuiTam Research Laboratory (Laboratory of Chemistry and Environmental Technologies – @quitam.ufv) at UFV-Florestal.

Leandro José dos Santos

Prof. Leandro holds both a Bachelor's and a Licentiate degree in Chemistry from the Federal University of Juiz de Fora (2004). Completed a Master's degree in Chemistry at the Federal University of Minas Gerais (UFMG, 2006), focusing primarily on the synthesis of carbohydrate and tetrazole derivatives. PhD in Chemistry from the UFMG (2010), working on the chemical modification and property studies of fullerene-C60. Conducted postdoctoral research in Chemistry at Université Grenoble Alpes (2019), focusing on methodologies for the synthesis of cyclic peptides and the development of molecules with potential biological activity. Currently, he is an Associate Professor at the Federal University of Viçosa – Florestal Campus.

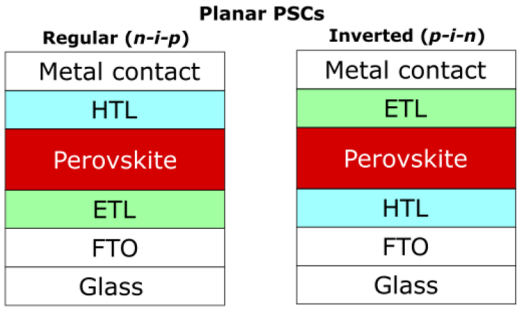

Fig. 1 Regular and inverted planar PSCs.

heterojunction devices. As an open-access tool, SCAPS-1D allows users to define a wide range of input parameters, such as bandgap values, carrier mobilities, doping concentrations, and defect densities, making it a practical resource to support the development and analysis of novel solar cell technologies.

While SCAPS-1D has been extensively adopted, it presents significant limitations in simulating optoelectronic devices, as it does not account for more complex physicochemical phenomena in materials, such as electrode behavior and interfacial reactions. It does include standard charge recombination mechanisms, such as Shockley–Read–Hall (SRH) recombination *via* bulk traps, radiative recombination, and Auger processes. However, it cannot model recombination phenomena coupled with ionic migration, interfacial electrochemistry, or degradation-related effects. Moreover, it does not consider chemical interactions, solvent effects, chemical and environmental degradation processes, or the influence of moisture in these devices. Furthermore, the software is limited to one-dimensional simulations and is not capable of modeling two or three-dimensional structures.[19]

For modeling multidimensional structures, simulation tools beyond SCAPS are required. For example, Liu *et al.* (2025)[20] employed Ansys Lumerical software implementing the finite-difference time-domain (FDTD) method to simulate PSCs with dual inverted pyramid architectures, using light trapping in both the FTO and the ETL (TiO_2). Similarly, Wang *et al.* (2025)[21] used COMSOL multiphysics to simulate PSCs featuring dual inverted pyramid structures at the HTL/perovskite and perovskite/ETL interfaces.

Despite the limitations mentioned previously, SCAPS-1D features an intuitive graphical user interface that is easy to learn and use, and it has significantly contributed to the understanding of photovoltaic mechanisms and the development and design of new thin-film solar cells, such as PSCs and organic solar cells (OSCs).[22]

Fig. 2 displays the main interfaces of the SCAPS-1D software used during the simulation process. Panel (a) shows the initial screen where the user defines the device structure and selects output parameters; panel (b) corresponds to the set problem screen, where the solar cell layers are configured and interface parameters are defined; and panel (c) presents the input screen for specifying physical and electronic parameters such as bandgap values, carrier mobility, and defect levels for each layer.

The insights provided by simulations are important for advancing research on PSCs. However, they should be interpreted with caution, as many studies have reported unrealistic results, including solar cell efficiencies that exceed the Shockley–Queisser limit, as pointed out by Saidarsan *et al.*(2025).[22] The authors emphasize the value of SCAPS-1D as a tool for identifying existing gaps and challenges in the commercialization of third-generation solar cells. Nevertheless, they stress that the simulation results should not always be interpreted as accurate representations of the real performance or potential of a device. These limitations arise from the fact that the results depend directly on how closely the input parameters reflect the experimental data, in addition to the specific approximations and numerical algorithms employed by SCAPS-1D.

Table 1 Experimental studies with lead-free PSCs

Experimental PSC	Method employed	Achieved efficiency (PCE) (%)	Reference
TiO_2/MASI/Spiro-MeOTAD (n–i–p)	Bandgap engineering	5.73	4
TiO_2/$CsSnI_3$/m-MTDATA (n–i–p)	Addition of SnF_2	2.02 with 20% of SnF_2 in $CsSnI_3$	6
(HTL-free) Meso. TiO_2/MASI with DMSO	Solvent engineering	3.15	7
Meso. TiO_2/$FASnI_3$/Spiro-MeOTAD (n–i–p)	Solvent engineering with SnF_2, pyrazine, DMF:DMSO	4.8	8
PEDOT:PSS/$FaSnI_3$/fullerene-C_{60} (p–i–n)	Addition of SnF_2, inverted configuration and solvent engineering	6.22	9
PEDOT:PSS/$FA_{0.98}EDA_{0.01}SnI_3$/C_{60} (p–i–n)	Passivation and post-treatment with the Lewis base ethane-1,2-diamine (edamine)	10.18	10
PEDOR:PSS/$(FA_{0.9}EA_{0.1})_{0.98}EDA_{0.01}SnI_3$/$C_{60}$ (p–i–n)	Bandgap and compositional engineering using ethylammonium iodide (EAI)	13.24	11
ITO/PEDOT:PSS/FASI + phenylethylamonium bromide (PEABr)/indene-C_{60} bisadduct (ICBA) (p–i–n)	Solvent engineering, one step method	14.6	5

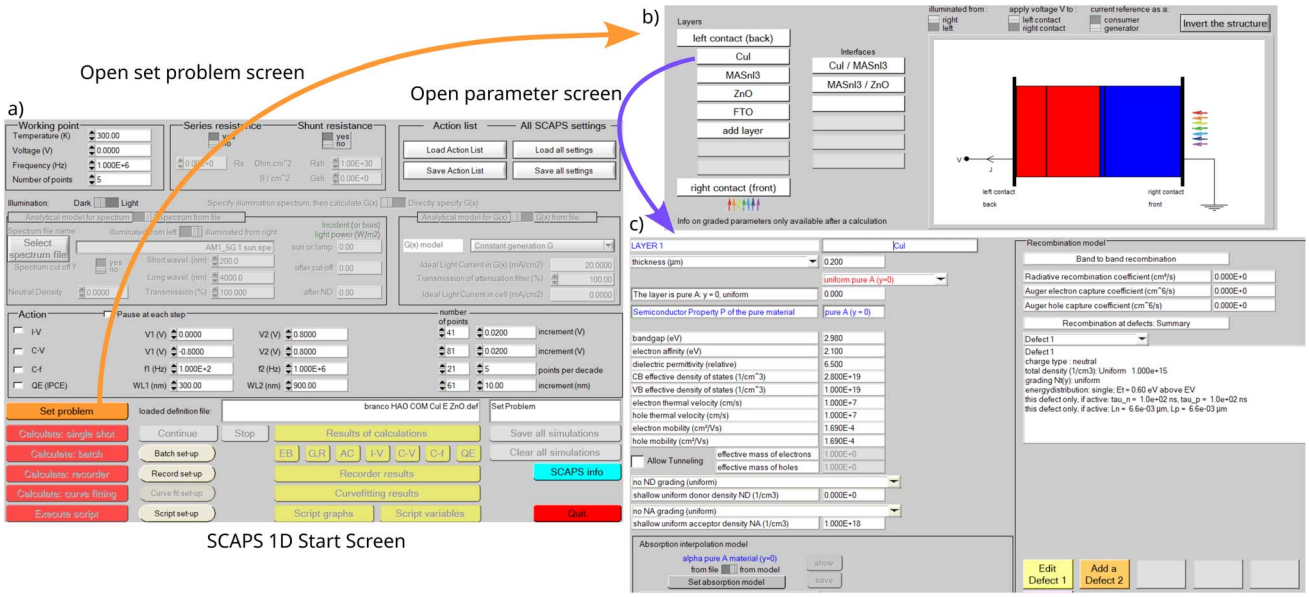

Fig. 2 Main SCAPS-1D interfaces used in the simulation setup: (a) initial screen of the SCAPS-1D software; (b) solar cell construction panel; (c) Input parameter configuration interface.

In recent years, research combining SCAPS-1D simulations with Machine Learning (ML) techniques to predict outcomes in perovskite solar cells (PSCs) has gained momentum. ML is a branch of Artificial Intelligence (AI) that enables machines to learn and make predictions based on data previously input by programmers, employing various types of algorithms.[23] ML has emerged as an alternative to traditional simulation and computational methods, such as density functional theory (DFT), which typically require substantial computational resources and long processing times. Moreover, such traditional methods are not particularly well-suited to studying the behavior of complex systems like PSCs.[24]

Machine learning is increasingly recognized as a powerful tool for supporting theoretical studies on PSCs by efficiently handling complex systems, reducing computational costs, and predicting the properties of unexplored devices using existing datasets. However, its application still faces key challenges. A major issue is data scarcity: most datasets are tabular, highly similar, and lack diversity (*e.g.*, image or text formats), which limits ML performance. Expanding these datasets typically requires time-consuming and costly methods, such as DFT. Another limitation is the credibility of the model. Although ensemble and deep learning algorithms offer higher accuracy, they often lack interpretability, making it difficult to understand how predictions are generated. Experimental validation could improve trust in these models, but also involves significant time and resources.[24,25]

Some examples of studies involving simulations of lead-free PSCs using SCAPS-1D combined with ML can be found in the work of Khan *et al.* (2025),[26] in which the authors simulated the Al/FTO/ZnS/$CH_3NH_3SnI_3$/MoO_3/Au PSC structure. Different parameters were adjusted to optimize photovoltaic performance, and an ideal defect density of 10^{14} cm^{-3} was assumed for the MASI perovskite. Afterwards, an ML model based on linear regression was used to analyze the influence of the physical parameters of the MASI on device efficiency, using a dataset of 740 samples. The coefficient of determination (R^2) was 0.878 for the training set, and the authors concluded that, according to the model, defect density was the most influential factor affecting the solar cell performance.

In another study, Shimul *et al.* (2024)[27] analyzed the performance of PSCs based on $CH_3NH_3SnBr_3$ as the perovskite absorber, V_2O_5 as the HTL, and different ETLs using both SCAPS-1D and wxAMPS. The best efficiency was achieved when WS_2 was employed as the ETL. The authors used a Random Forest algorithm to evaluate whether the machine could accurately predict the output parameters based on the inputs generated by the 1D simulation software. High R^2 values were obtained, particularly for PCE (0.87), along with an overall model precision of 82%.

Finally, Khan and Ahmed (2024)[28] simulated the Al/FTO/WS_2/FASnI$_3$/Zn_3P_2/Ni PSC using SCAPS-1D and used the simulation results as a dataset for training an ML model. The goal was to assess the impact of various parameters (thickness, bandgap, electron affinity, acceptor density, and defect density) on device performance. Using Neural Designer ML software and 243 samples, the study again identified defect density as the primary factor that influences photovoltaic performance.

Although there are some literature reviews on PSC modeling,[19,22,29–31] none focus exclusively on lead-free PSCs modeled with SCAPS-1D. In this context, the present work provides a recent review of simulation studies on lead-free PSCs modeled with SCAPS-1D using B-site metals such as tin, germanium, and manganese, among others. Our work covers publications from 2016 to 2025 and also highlights performance improvements reported in these studies. Finally, this

review is organized into two parts: PSCs simulated with tin (Section 2.1), and PSCs with other metals substituted at the perovskite B-site (Section 2.2).

2 Lead-free PSCs simulations

2.1 PSCs using Sn as the B-site metal in the absorber material

Tin-based perovskites offer not only a less toxic alternative to lead at the B-site, but also optoelectronic properties favorable for PSC applications. For example, MASI perovskite surpasses MAPI in terms of charge carrier mobility and UV-visible light absorption, as highlighted by Hasnain (2023).[32]

Despite these favorable characteristics, one of the main challenges in working with tin-based PSCs is their rapid oxidation to Sn^{4+}, resulting in ineffective incorporation of Sn into the crystal lattice. This oxidation process leads to poor film homogeneity, and consequently to the generation of defects that reduce both the efficiency and stability of the device. Furthermore, tin-based solar cells are not considered entirely safe for the environment, as their low stability can result in the formation of unstable degradation products, such as SnI_2, which rapidly decomposes into hydroiodic acid (HI).[33]

Other challenges associated with Sn-based PSCs include moisture-induced degradation, since the organic cations in MASI and FASI perovskites are hygroscopic and readily degrade in the presence of water. Although inorganic cations such as Cs are not entirely immune to this instability, using alternative inorganic cations could help mitigate moisture-induced degradation. Temperature effects can also trigger phase transitions in tin-based perovskites. Finally, similar to Pb-based PSCs, light-oxygen-induced degradation leads to perovskite deterioration and an increase in iodine vacancy density.[34]

A key limiting factor in the commercialization of Sn-based PSCs is the instability of these devices resulting from oxidative stress. Encapsulation processes are crucial to address this issue, and research on proper encapsulants is essential for the advancement of the field, as highlighted by Aktas *et al.* (2022).[34] Although encapsulation is one of the main strategies for mitigating degradation caused by moisture and exposure to ambient air, these agents can still slowly penetrate the PSC. Furthermore, the encapsulant itself degrades over time. In this scenario, interface engineering also emerges as a key approach to improving the long-term stability of PSCs, as hydrophobic interlayers can act as additional moisture barriers, complementing encapsulation.[35]

Several experimental approaches have also been employed to address the stability challenges of tin-based PSCs. Among the most prominent strategies are the incorporation of additives, such as SnF_2, into the light absorbing layer to enhance the crystallization of the perovskite film and reduce defects, as well as composition engineering at the perovskite cationic site.[36]

Consequently, both experimental and computational studies have been conducted to address the low stability of tin-based perovskites. In the following section, we discuss simulation studies specifically focused on perovskites incorporating tin at the B-site of the crystal structure.

2.1.1 Composition and interface engineering in PSCs. Composition engineering is one of the methods used to enhance the performance and stability of PSCs. This technique can be applied to various layers through doping and material modification, aiming not only to optimize their physicochemical and optoelectronic properties but also to improve the morphology and chemical stability of the films. Specifically, in the absorber layer, composition engineering enables adjustment of the tolerance factor of the ABX_3 perovskite. This parameter predicts the structural stability of the material based on the ionic radii of its constituent elements, achieved by substituting or incorporating new elements into perovskite sites.[37]

With respect to interface engineering, it is a strategy aimed at reducing non-radiative recombination, passivating surface defects, and improving both band alignment between materials and charge transport and collection.[35] This engineering approach can be applied at various interfaces, such as HTL/perovskite, ETL/perovskite, and ETL(or HTL)/electrode, depending on the device configuration.[38]

This section analyses studies employing either composition engineering or interface engineering strategies in lead-free tin-based PSCs. Compared to studies on composition engineering, fewer SCAPS-1D simulation studies investigating interface engineering were found in this review.

Jalalian *et al.* (2019)[17] studied the performance of an HTL-free PSC using the perovskite $CH_3NH_3SnI_{3-x}Br_x$, where the halide concentration at the X site was varied, with a defect density (N_t) of the absorber layer of 4.5×10^{17} cm^{-3}. It was observed that as the bromide concentration in the perovskite increased, the V_{oc} and the fill factor (FF) also increased due to a reduced charge recombination rate, while the J_{sc} decreased. The PCE of the solar cell also decreased after the bromide proportion x exceeded 1. The authors concluded that a uniform bandgap in the perovskite absorption layer may not be ideal for Pb-free PSCs. A viable alternative for materials with variable bandgaps, such as the perovskite they studied, is the bandgap gradient, a concept initially applied to improve the power conversion efficiency (PCE) of copper–indium–gallium–selenium (CIGS) thin-film solar cells.

The authors employed the double leveling method to achieve this variable bandgap, dividing the absorber layer into multiple sublayers within the simulation software. Different bandgap values were assigned to each sublayer according to the desired concentrations. Fig. 3 schematically illustrates a typical trapezoidal bandgap profile inspired by the concept described by Jalalian *et al.* (2019).[17] Finally, tuning the bromide content (x) varied the bandgap between 1.5 and 2.3 ev. A maximum PCE of 16.30% was achieved at x for 1.13.

Gamal *et al.* (2021)[39] simulated an n–i–p PSC using MASI as the light-absorbing layer, $CH_3NH_3SnBr_3$ as the HTL, and $Zn_{1-x}Mg_xO$ as the ETL, where ETL composition engineering was applied to enhance device performance. $Zn_{1-x}Mg_xO$ was chosen as the ETL instead of TiO_2 due to its tunable bandgap. The increase in Mg concentration also widened the ETL bandgap, allowing more sunlight to be transmitted in the UV range. Thus,

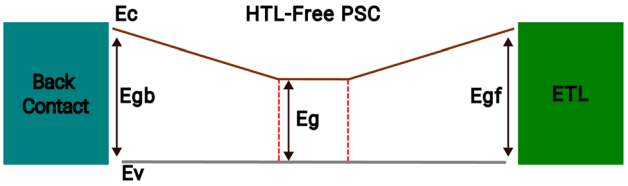

Fig. 3 Schematic illustration of a trapezoidal bandgap profile showing the ETL, graded absorber back region (E_{gb}), absorber front region (E_{gf}) and conduction and valence band (E_v and E_c). Inspired by Jalalian *et al.* (2019).[17]

the best performance was obtained using a Mg proportion of 0.25, reaching a PCE of 17.09%, when a N_t of 1×10^{16} cm^{-3} was used in the MASI perovskite.

Salem *et al.* (2021)[13] constructed a hybrid homo-heterojunction PSC using a homojunction of both n-type and p-type MASI perovskites (Fig. 4). Although the authors refer to the baseline device in their work as a "conventional pin structure", the architecture presented, FTO/TiO_2/perovskite/Spiro-OMeTAD, clearly corresponds to an n–i–p configuration, where light enters through the ETL (TiO_2). According to the authors, this was the first simulation study of homojunction PSCs using lead-free perovskites, as previous studies had focused exclusively on MAPI-based devices. Compared to heterojunction solar cells, a homojunction cell generates a stronger electric field that can assist the effective transport of electrons and holes, thereby reducing charge recombination losses. In the study, the authors considered a realistic defect density with a value of 5×10^{17} cm^{-3}.

The influence of the thicknesses and doping concentrations of the n-MASI and p-MASI absorber layers was evaluated. The thickness of p-MASI ranged from 0 to 350 nm, always maintaining the sum of the two layers at 350 nm. There was an increase in the values of all output parameters, including the efficiency of the solar cell, with the increase of the p-MASI thickness up to 300 nm, thus optimizing the homojunction at 300 nm of p-MASI and 50 nm of n-MASI. After optimization of other factors, such as the N_A doping values in p-MASI and N_D in n-MASI, the simulated hybrid cell achieved an efficiency of 8.66%.

Subsequently, an HTL-free PSC was simulated to study the influence of different ETLs, various electrodes, and changes in doping and defect density. The band alignment between the ETL and the absorber was evaluated by varying the ETL materials (Fig. 5) and calculating the conduction band offset (CBO), a measure of the conduction band mismatch between the ETL and the perovskite. It was observed that when using TiO_2, the CBO resulted in a negative value, causing a cliff between the bands that did not inhibit the flow of photogenerated electrons to the front electrode. However, charge recombination at the interface increased in this case because the activation energy for carrier recombination (E_a) became lower than the perovskite bandgap.

When ZnO and [6,6]-phenyl-C_{61}-butyric acid methyl ester (PCBM) were used as ETLs, the CBO presented a positive value, resulting in a spike between the interfaces, and $E_g = E_a$. When this peak is small enough, it does not impede the flow of electrons. However, when it exceeds 0.2 eV, the electron flow is directly affected, leading to a drastic decrease in output parameters such as FF and efficiency. In this context, the best PCE of 9.35%, was obtained using ZnO as ETL and a high defect density in perovskite layer (10^{17} cm^{-3}). When an ideal N_t value was used, 19.37% efficiency was achieved.

Considering the stability challenges associated with PSCs that employ FASI as the absorber layer, particularly oxidation and deviations in crystal structure, Sabbah *et al.* (2022)[40] investigated the incorporation of cesium into formamidinium tin iodide perovskites ($FA_{1-x}Cs_xSnI_3$) in regular configuration. They compared their performance with devices simulated using undoped FASI. The authors evaluated different FA/Cs ratios, replacing TiO_2 with ZnOS as the ETL while maintaining Cu_2O as the HTL, and fixed N_t at 1×10^{15} cm^{-3} for the absorber layer.

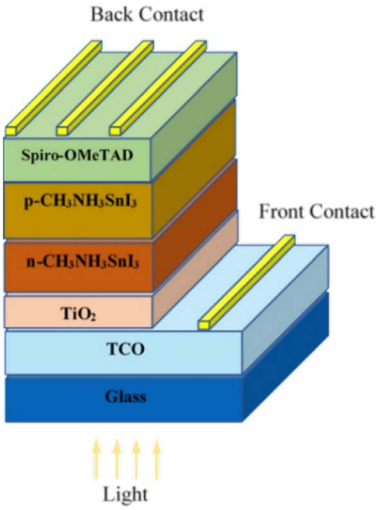

Fig. 4 Lead-free hybrid hetero-homojunction perovskite solar cell. Reproduced from Salem *et al.* (2021)[13] (https://doi.org/10.3390/en14185741). © 2021 by the authors. Licensed under CC BY 4.0.

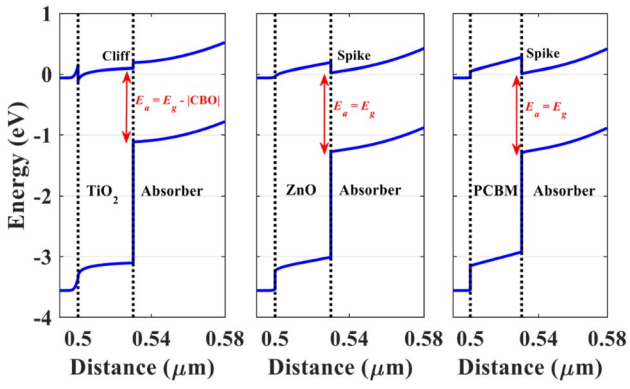

Fig. 5 Band alignment between the perovskite absorber and different ETLs, illustrating cliff and spike profiles. Reproduced from Salem *et al.* (2021)[13] (https://doi.org/10.3390/en14185741). © 2021 by the authors. Licensed under CC BY 4.0.

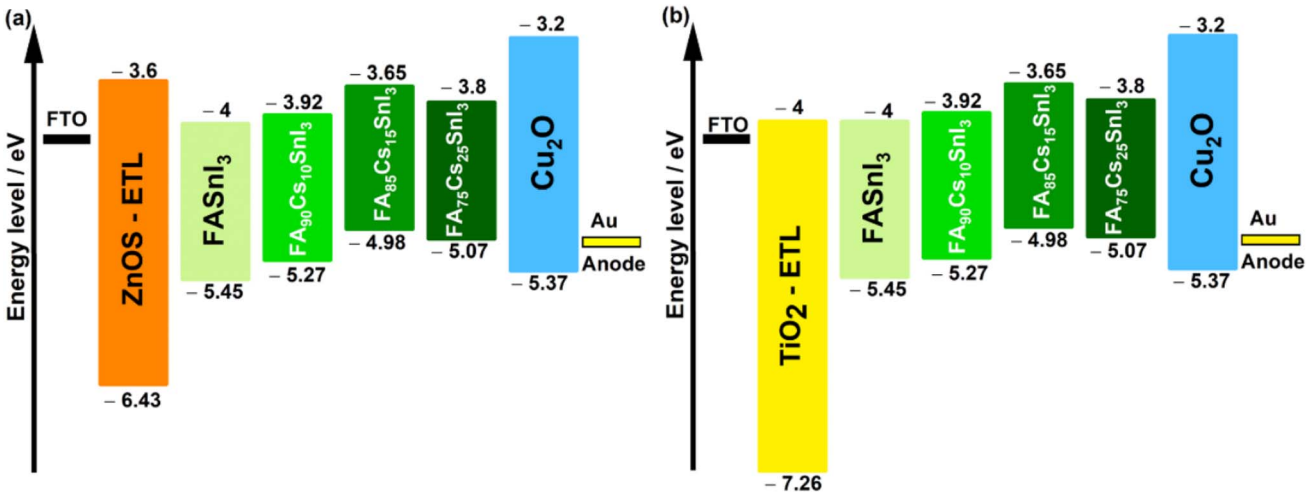

Fig. 6 Band alignment between FASI perovskites with different cesium contents and the ETLs TiO_2 (a) and ZnOS (b). Reproduced from Sabbah *et al.* (2022),[40] (https://doi.org/10.3390/ma15144761). Licensed under CC BY 4.0.

Fig. 6, reproduced from their study, presents the band alignments between the various perovskites and the ETLs. All configurations using ZnOS as ETL outperformed those using TiO_2, a result attributed to the lower electron mobility of TiO_2 (20 $cm^2\ V^{-1}\ s^{-1}$) compared to perovskites (22 $cm^2\ V^{-1}\ s^{-1}$), leading to higher recombination rates in this ETL. The calculated CBO between ZnOS and the perovskites remained positive across all Cs concentrations, resulting in an interfacial spike that enhanced device performance. In contrast, the CBO for the FASI/TiO_2 interface decreased with increasing Cs content, becoming negative and contributing to a drop in PCE from 12.1% to 3.41% (considering 15% Cs content). Upon optimizing parameters such as N_t and N_A, the authors reported a maximum efficiency of 22% using $FA_{0.75}Cs_{0.25}SnI_3$.

Ferhati *et al.* (2023)[41] adopted the bandgap variation technique, as previously demonstrated by Jalalian *et al.* (2019).[17] The authors referred to this method as the graded bandgap (GBG) approach. In their work, the bandgap values of the ETL were varied by testing materials such as Zn(S,O), ZnMgO, and the perovskite $CsFaSnI_3$, used as the absorber layer. PEDOT:PSS was employed as the HTL in PSCs with an n–i–p architecture. The cesium concentration was varied for the perovskite to achieve an optimal GBG, while the magnesium and oxygen concentrations were adjusted in the ETL to improve band alignment.

When comparing the current density–voltage curves (*J–V* curve) of the proposed solar cell (C_{60}/GBG-FACsSnI_3) with a cell lacking GBG in the absorber layer (C_{60}/FASI), an increase in current density was observed, attributed to Cs doping, together with improved charge generation and reduced recombination losses. This improved performance was linked to the variable bandgap at the ETL/perovskite interface, enabling energy level balancing and optimizing the photogeneration mechanism.

Building on this improvement, the authors also applied the GBG approach to the tested inorganic ETLs, which demonstrated better performance than the C_{60} ETL. Band alignment analysis reveals the formation of a peak at the Zn(S,O)/perovskite interface, whereas a cliff forms at the ZnMgO/perovskite interface. The presence of this cliff can increase charge recombination. Nevertheless, the device with the GBG-ZnMgO ETL exhibited better performance than the one based on fullerene-C_{60}. Specifically, the GBG-Zn-(O,S)/GBG-FACsSnI_3 PSC achieved an efficiency of 21.67%, compared to 16.78% for the C_{60}/GBG-FACsSnI_3 PSC and 19.51% for the GBG-ZnMgO/GBG-FACsSnI_3 configuration. The authors used a neutral defect density of 10^{14} cm^{-2} in both ETL/perovskite and HTL/perovskite interfaces, but did not report the defect density value assumed for the perovskite layer, which compromises a realistic assessment of the results obtained.

Sajid *et al.* (2023)[42] simulated and constructed a homojunction-based HTL-free PSC with FTO/TiO_2/$FASnI_3$/$CsSnI_3$/Au configuration. $FASnI_3$/$CsSnI_3$ perovskites were used as the light-absorbing layer due to their similar crystal structure, which can provide a film with higher quality and lower defect density. The N_t used was considered real in both perovskite layers: 1×10^{16} cm^{-3} in the $FASnI_3$ layer and 1×10^{15} cm^{-3} in the $CsSnI_3$ layer. The authors explored the thickness of the $CsSnI_3$ layer, due to its significant influence on light absorption and charge generation. From the simulations, it was observed that the solar cell efficiency increased with thickness up to 400 nm. However, the authors opted to maintain a thickness of 100 nm due to constraints in assembling the experimental device, as the precursor solvent of the $CsSnI_3$ perovskite dissolves the underlying $FASnI_3$ layer, limiting the feasible thickness. Consequently, the theoretical results reached 0.78 V, 27.65 mA cm^{-2}, 79.74% and 19.03% for the output parameters V_{oc}, J_{sc}, FF and PCE, respectively.

For the experimental fabrication of the PSC, a one-step method was employed to incorporate FASI, while a two-step method was used for $CsSnI_3$. The authors fabricated two PSCs with the configurations of FTO/c-TiO_2/m-TiO_2/$FASnI_3$/Au and FTO/c-TiO_2/m-TiO_2/$FASnI_3$/$CsSnI_3$/Au, using compact and mesoporous TiO_2 layers. The PSC using the $FASnI_3$/$CsSnI_3$

homojunction achieved better results, reaching 0.84 V, 22.06 mA cm^{-2}, 63.50% and 11.77% for V_{oc}, J_{sc}, FF and PCE values, respectively, when compared to the PSC using only FASI as absorber layer (0.79 V, 21.20 mA cm^{-2}, 53.35% and 8.94% for V_{oc}, J_{sc}, FF and PCE). Although the efficiency reported in the simulation study was significantly higher than the experimental results, it was evident that incorporating the $CsSnI_3$ in the perovskite layer contributed to an improved device performance compared to PSCs using only $FASnI_3$.

Our previous study[43] simulated PSCs using fullerene-C_{60} and its PCBM derivative as interlayers in both regular and inverted device architectures, based on the CuI/MASI/ZnO structure, as shown in Fig. 7. The objective was to evaluate the influence of fullerene derivatives on enhancing the performance of lead-free PSCs through the interface engineering method.

Using a high defect density (N_t) of 4.5 × 10^{17} cm^{-3}, it was observed that the inclusion of PCBM as an interlayer positively influenced the efficiency of the solar cell, compared to unmodified fullerene (C_{60}). This improvement was attributed to the energy level misalignment between the MASI perovskite and C_{60}, which likely promoted charge recombination. The incorporation of PCBM increased the PCE of the n–i–p device from 6.90% to 8.11%, and of the inverted structure (iPSC) from 3.72% to 5.26%. Using a lower defect density of 4.5 × 10^{16} cm^{-3}, PCE further improved to 13.38% and 10.00% for the n–i–p and p–i–n configurations, respectively, as shown by the *J–V* curves in Fig. 8.

Khan *et al.* (2024)[44] investigated the influence of graphene as a passivation layer between FASI perovskite with 5% Zn doping and the Cu_2O HTL in a regular-structure PSC. By varying the bandgap of graphene from 1.7 to 2.2 eV, the device efficiency increased from 12.36% to 13.23%. It was observed that, as the bandgap increased, the interfacial energy barrier decreased, with an optimal value of 1.9 eV leading to the best performance across all output parameters. After further optimizations of the FASI:Zn absorber layer, the authors achieved a PCE of 21.17%, using an ideal N_t value (10^{13} cm^{-3}).

2.1.2 Influence of the ETLs/HTLs on PSCs. The electron and hole transport layers play an essential role in the efficient functioning of the solar cell. Their intrinsic properties, such as high charge mobility and proper alignment of energy levels with those of the perovskite, are essential to ensure good device performance.

The HTL, in particular, faces challenges related to stability, which can compromise the overall efficiency of PSCs. Organic HTLs currently present the highest efficiencies, but their use often requires incorporating additives to enhance charge mobility and stability because they are more prone to degradation. On the other hand, inorganic HTLs, although considered more stable and cost-effective, generally exhibit lower efficiency compared to their organic counterparts and often require more expensive and complex techniques during the deposition stage of the solar device.[45]

Khattak *et al.* (2019)[46] simulated n–i–p PSCs using perovskite MASI as the absorber layer. Different quaternary compounds Cu_2XSnY_4 (or CXTY) were used as HTLs, with site X occupied by elements such as Zn, Fe, Ni, Ba, and Mn, and site Y by S and Se. Among the HTLs used in the study, copper zinc tin selenide ($Cu_2ZnSnSe_4$ or CZTSe) achieved the highest efficiency of 19.43% when an ideal N_t to MASI was considered.

Abdelaziz *et al.* (2020)[47] investigated, for the first time, by solar cell simulations, the use of FASI perovskite as the absorber layer in a PSC with p–i–n configuration. Initially, Spiro-MeOTAD and TiO_2 were used as HTL and ETL, respectively. The N_t of the perovskite layer was set at 1 × 10^{15} cm^{-3}. The influence of using CuI, Cu_2O, and NiO as HTLs, and ZnO and ZnSe as ETLs was investigated. With TiO_2 maintained as the ETL and various HTLs tested. In contrast, when Spiro-MeOTAD was used as the HTL and the ETLs were varied, the device reached a PCE of 3.80% using ZnO as the ETL. After further optimizations, particularly in absorber doping, the authors achieved a PCE of 14.03%.

Deepthi Jayan and Sebastian (2021)[12] investigated the performance of MASI-based PSCs in the conventional n–i–p configuration, using different types of ETLs, HTLs, and metallic contacts, with an ideal N_t value of 2.5 × 10^{13} cm^{-3}. With regard to the metallic contacts, the authors observed that the PCE increased with the work function of the metals, which they attributed to the absence of chemical reactions between the

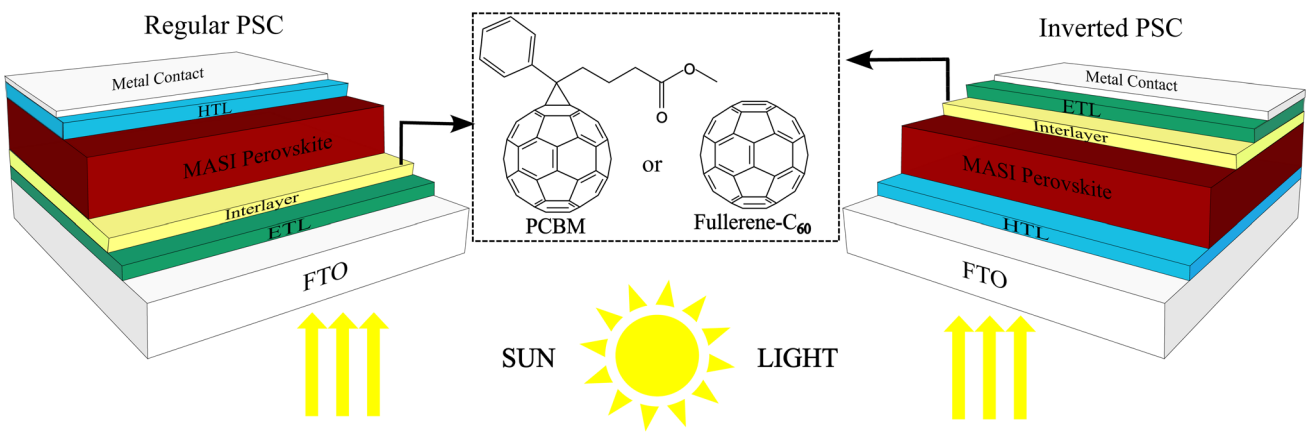

Fig. 7 Fullerene-C_{60} and its derivative PCBM used as interlayers in MASI-PSCs with CuI/MASI/ZnO architecture. Reproduced from Araújo *et al.* (2024)[43] (https://doi.org/10.1039/D4RA00634H) under a CC BY 4.0 license.

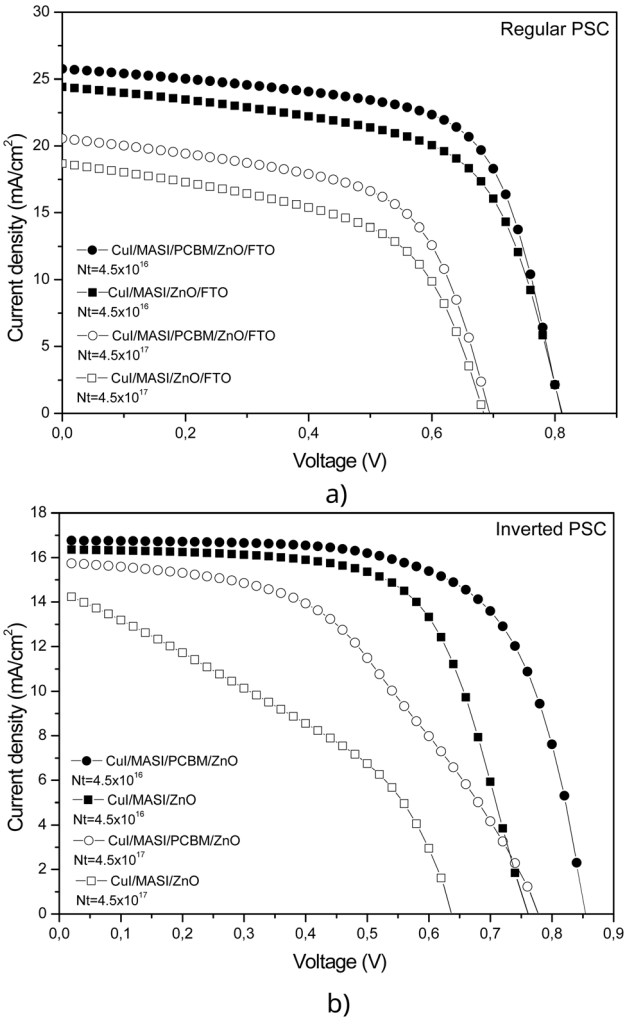

Fig. 8 *J–V* curves for n–i–p (a) and p–i–n (b) PSCs with and without the use of PCBM as an interlayer, using N_t values of 4.5×10^{16} (open symbols) and 4.5×10^{17} (filled symbols). Reproduced from Araújo *et al.* (2024)[43] (https://doi.org/10.1039/D4RA00634H) under a CC BY 4.0 license.

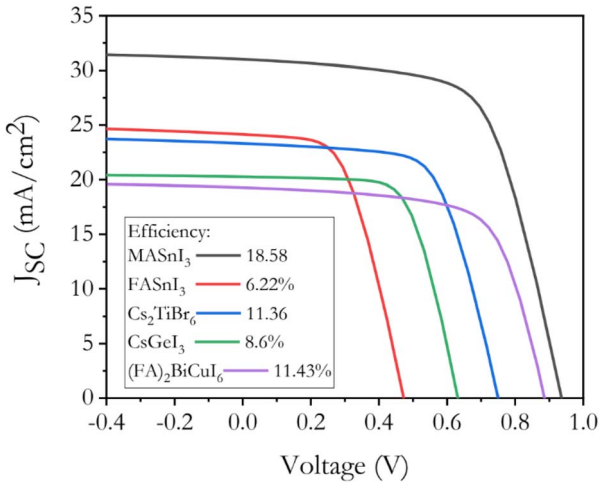

Fig. 9 *J–V* curves of the PSCs comparing different lead-free perovskites using CZTS as the HTL. Reproduced by Reyes *et al.* (2021)[48] (doi:https://doi.org/10.3390/mi12121508) under a Creative Commons Attribution (CC BY 4.0) license.

perovskite layer and these metals. In contrast, metals with low work functions, such as silver, were found to react chemically with the perovskite, negatively impacting the device efficiency. PCBM and CuI were identified as the best performing ETL and HTL, respectively, with the FTO/PCBM/$MASnI_3$/CuI/Au configuration achieving the highest PCE of 25.05%.

Reyes *et al.* (2021)[48] evaluated the influence of copper–zinc and tin sulfide, Cu_2ZnSnS_4 (CZTS), as HTL in an n–i–p PSC using MASI. Based on a compilation of simulation data from various studies involving different lead-free perovskites, the authors constructed comparative *J–V* curves shown in Fig. 9. These data indicate that MASI demonstrated superior performance with an efficiency of 18.58%, while other materials such as FASI showed significantly lower efficiencies (6.22%). However, the authors did not report the defect density values used in the individual compiled studies and did not consider this parameter in their comparison, which may compromise the validity of directly comparing the efficiencies. MASI was selected over other lead-free perovskites due to its comparatively better performance in these compiled simulations. The new device constructed by the authors achieved an efficiency of 20.28% after implementing optimizations such as adjustments to the thickness of the MASI perovskite and the HTL, using an ideal N_t of 1×10^{14} cm^{-3}.

Das *et al.* (2022)[49] simulated regular PSCs using MASI perovskite with different HTLs. The authors aimed to understand how organic and inorganic HTLs influenced solar cell performance. To this end, they used Spiro-MeOTAD and PEDOT:PSS as organic HTLs and CuO and Cu_2O as inorganic HTLs. Using an ideal N_t, the difference in PSC efficiency with different HTLs was insignificant, varying less than 1%.

Mushtaq *et al.* (2023)[50] evaluated the use of different HTLs (Cu_2O, $CuSbS_2$, CuI, NiO, and Spiro-MeOTAD) and ETLs (SnO_2, TiO_2, WS_2, CdS, and ZnO) in a lead-free PSC with an n–i–p structure, using $MASnBr_3$ as the absorber layer. Fixing TiO_2 as the ETL, the highest PCE (29.21%) was obtained when NiO was used as the HTL. With NiO selected as the HTL, the authors proceeded to vary the ETL. Although the differences in output parameters were not significant, a slightly higher PCE was observed when SnO_2 was used. After the transport layers were defined, additional parameters such as the doping density of the absorber and the thicknesses of all layers were optimized.

It should be noted that the simulations assumed ideal defect densities for all layers, including the ETLs, HTLs, and the $MASnBr_3$ absorber, with values ranging between 10^{14} and 10^{15} cm^{-3}. In relation to the absorber, the influence of N_t was analyzed, varying it between 10^{12} and 10^{18} cm^{-3} and the best performance was achieved with a defect density of 10^{14} cm^{-3}. After optimizations in layer thickness, the highest performance was obtained with a PCE of 34.52% and a FF of 88.30%.

Hossain *et al.* (2023)[51] investigated strategies to improve the efficiency of PSCs in the n–i–p configuration, using cesium tin chloride ($CsSnI_3$) as the absorber material and PCBM as the

ETL. The study evaluated various HTLs (CuSCN, NiO, P3HT, PEDOT:PSS, Spiro-MeOTAD, CuI, and CFTS) and metallic contacts (Au, W, Ni, Pd, Pt, Se, Ag, C, Fe, and Cu). After identifying the most effective layer combination, the authors optimized the thickness and defect density parameters. The ITO/PCBM/$CsSnI_3$/CFTS/Se configuration outperformed all others, achieving an efficiency of 24.73% following all optimizations, with an ideal N_t of 1×10^{13} cm^{-3} for the perovskite layer. The second best PCE, 12.96%, was obtained with the ITO/TiO_2/$CsSnI_3$/Spiro-MeOTAD/Au configuration.

The same research group[52] investigated the use of $CsSnCl_3$ as the absorber material in PSCs with the n–i–p configuration, evaluating 96 different simulated configurations by testing various ETLs and HTLs to identify the optimal conditions for device performance. The N_t was fixed in 1×10^{15} cm^{-3}. The ETLs tested included fullerene-C_{60}, PCBM, indium–gallium–zinc–oxide (IGZO), SnO_2, WS_2, CeO_2, TiO_2, and ZnO, while the materials used as HTLs were Cu_2O, CuO, NiO, V_2O_5, CuI, CuSCN, $CuSbS_2$, Spiro-MeOTAD, P3HT, PEDOT:PSS, copper barium thiostannate (CBTS), and Cu_2FeSnS_4 (CFTS).

The authors observed that the band alignment between the perovskite and the CBTS HTL was the most favorable among all HTLs tested, leading to its selection for subsequent evaluations with different ETLs. In terms of the ETLs, fullerene-C_{60} and PCBM exhibited poor band alignment, as illustrated in the adapted graph (Fig. 10), while compounds such as ZnO and TiO_2 demonstrated better alignment and overall performance. The device with ITO/TiO_2/$CsSnCl_3$/CBTS/Au configuration achieved an efficiency of 21.75% and 82.03% of FF. Finally, the authors also used DFT calculations to further investigate the structural, electrical, and optical characteristics of the $CsSnCl_3$ absorber.

AlZoubi *et al.* (2024)[53] synthesized a HTL-free PSC using FASI as the absorber layer and C_{60} fullerene as the ETL, aiming to explore the viability of HTL-free architectures under ideal defect density conditions (1×10^{14} cm^{-3}). The authors also simulated a reference device including an HTL (PEDOT:PSS) and compared its output parameters (V_{oc}, J_{sc}, FF, and PCE) with those of the HTL-free PSC. All performance parameters improved with removal of the HTL, particularly the FF, which increased from 78.25% to 82.09% and the PCE, which increased from 12.53% to 14.46%. When varying the thickness of the C_{60} ETL from 10 to 200 nm, a performance decline was observed for thicknesses greater than 50 nm. After further optimizations, the authors achieved a final efficiency of 19.63%.

Singh *et al.* (2024)[54] investigated the use of different HTLs and ETLs in a lead (Pb)-free ethylammonium (EA)-substituted ethylenediamine (EDA)-based PSC, with the composition $[(FA_{0.9}EA_{0.1})_{0.98}EDA_{0.01}SnI_3]$, in a regular configuration. The baseline simulated PSC employed Cu_2O as the HTL and PCBM as the ETL, achieving a PCE of 21.87% when a defect density (N_t) of 1×10^{14} cm^{-3} was used in the absorber layer. Keeping Cu_2O as the HTL and varying the ETLs, the simulated devices using unmodified fullerene-C_{60} and gallium(II) selenide (GaSe) as the ETLs showed the poorest photovoltaic performance. The misalignment between the conduction bands of the ETLs and the work function of the front contact, when these ETLs were used, was one of the main reasons for these results. The use of C_{60} resulted in a PCE of only 7.14%. The best performance, reaching 22.19%, was obtained when zinc oxysulfide (ZnOS) was used as the ETL, due to its better band alignment compared to the other tested materials and its high charge carrier mobility.

Regarding HTLs, while keeping ZnOS as the ETL, the device employing arsenic(III) telluride (As_2Te_3) as the HTL showed the worst performance, which the authors attributed to its limited built-in potential (V_{bi}). In contrast, the PSC simulated with copper(II) phthalocyanine (CuPc) as the HTL achieved favorable output parameters and an efficiency of 22.36%. After optimizing the perovskite thickness to 1100 nm, the device reached a final PCE of 24.42%.

2.1.3 Influence of adjustable parameters on PSC performance: thickness, doping concentration, and defect density. As previously demonstrated, the perovskite composition and the selection of charge transport layers significantly impact PSC performance. However, other factors also play a crucial role in enhancing the device's output parameters, particularly the morphology and crystallinity of the perovskite film. Poor crystallinity leads to an increased defect density, which directly

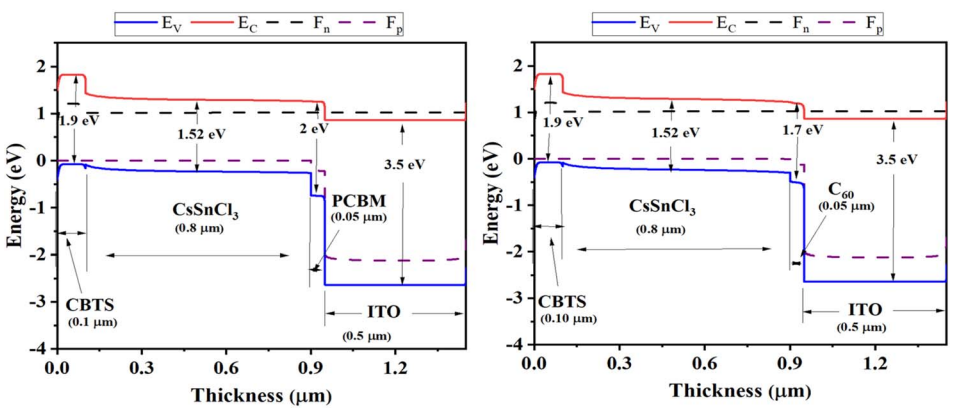

Fig. 10 Band diagrams of PSCs using PCBM and C_{60} as ETLs. Reproduced and adapted from Hossain *et al.* (2023)[52] (doi: https://doi.org/10.1038/s41598-023-28506-2) under a Creative Commons Attribution (CC BY 4.0) license.

contributes to non-radiative recombination losses and reduces both efficiency and operational stability. Therefore, parameters such as defect density in the functional layers and doping concentration must be carefully optimized to enhance charge transport and minimize recombination pathways in lead-free PSCs.[55]

Layer thickness in PSCs also plays a critical role in device optimization. For the absorber layer, increasing the thickness improves light absorption, but beyond a certain point, it promotes charge recombination. In contrast, excessively thin layers result in insufficient light absorption, thereby reducing device efficiency.[56,57] ETLs can be fabricated as thinner layers because they exhibit moderate electrical conductivity and have a low tendency to form defects during deposition. However, in p–i–n PSCs, the ETL thickness must be sufficient to prevent direct contact between the perovskite and the metal electrode.[58] For HTLs, particularly organic types, thicker layers are necessary due to their low conductivity and high susceptibility to defects and pinholes, which negatively impact solar cell performance.[59]

Du *et al.* (2016)[16] studied for the first time the effects of changes in dopant concentration and defect density in the absorber layer of lead-free PSCs using MASI in the n–i–p configuration through simulations in SCAPS-1D. Due to the tendency of Sn^{2+} ions to oxidize into Sn^{4+}, which causes unintentional p-type doping in the absorber layer, the authors investigated the effect of varying the acceptor density (N_A) from 10^{14} to 10^{17} cm^{-3}. For N_A concentrations below 1×10^{16} cm^{-3}, the PSC achieved an optimized efficiency of 8.03%. However, the recombination rate increases at higher doping levels, significantly decreasing the PCE. The study also evaluated the influence of defect density (N_t) on PSC performance, varying it from 10^{14} to 10^{19} cm^{-3}. In these lead-free PSCs, a similar trend to that observed in lead-based PSCs was found: reducing N_t positively impacts device efficiency by mitigating non-radiative recombination.

Lazemi *et al.* (2018)[60] studied the influence of CuSCN as the HTL in an n–i–p MASI-based PSC. The study showed that V_{oc} is more sensitive to defect density (N_t) variations than J_{sc}. The best efficiency of 26.05% was obtained using an N_t of 4.5×10^{16} cm^{-3} in the absorber layer.

Kumar *et al.* (2020)[14] investigated how changes in various parameters could improve solar cell performance in an n–i–p PSC, using FASI as the light absorber layer, TiO_2 as the ETL, and Spiro-MeOTAD as the HTL. The N_t value was varied between 10^{14} and 10^{16} cm^{-3}, achieving an optimized PCE value of 9.39% when a N_t of 10^{15} cm^{-3} was used. It also evaluated how variation in the values used for doping the absorber can influence the output parameters of the solar cell. An optimized efficiency of 10.90% was also achieved with a doping concentration of 10^{15} cm^{-3}.

Sunny *et al.* (2021)[61] evaluated the performance of an HTL-free PSC using MASI as the absorber and TiO_2 as the ETL by varying several factors, including the absorber doping density. The N_t used in the absorber layer was 10^{14} cm^{-3}. The output parameters remained nearly constant up to a doping concentration of 10^{15} cm^{-3}. Beyond this value, V_{oc}, FF, and PCE increased, while J_{sc} decreased.

Singh *et al.* (2024)[62] studied the influence of N_t that varied between 1×10^{13} cm^{-3} and 4×10^{15} cm^{-3} in a regular PSC with the FTO/SnO_2/$FASnI_3$/CuI/Au configuration. The authors obtained as output parameters a V_{oc} of 1.28 V, a J_{sc} of 27.72 mA cm^{-2}, an FF of 85.33% and an efficiency of 30.33% when using a thickness of 450 nm of FASI perovskite and a defect density considered ideal (1×10^{13} cm^{-3}).

As previously highlighted, the optimization of layer thickness is crucial for achieving a balance between light absorption and charge extraction in PSCs. Thickness engineering approaches have been applied to adjust the absorber, ETL, and HTL layers, resulting in improved device efficiencies through controlled adjustments.[31] Therefore, precise optimization is required to balance light absorption and charge extraction.

Shamna *et al.* (2020)[63] evaluated how the thickness of the MASI perovskite, the ETL (PCBM) and the HTL (NiO) affects the overall performance of the simulated PSC in the inverted p–i–n configuration, using an ideal N_t (1×10^{14} cm^{-3}). As the thickness of the MASI perovskite increased from 200 to 600 nm, the PCE of the solar cell also increased, reaching a maximum of 22.95% at 600 nm, but efficiency decreased at thicknesses beyond this value. However, the FF and the V_{oc} values decreased with increasing thickness. The authors noted that varying the ETL and HTL thicknesses did not significantly affect the output parameters.

Yasin *et al.* (2021)[64] simulated an n–i–p PSC using MASI perovskite as both the hole-absorbing and hole-transporting layers, and $CH_3NH_3SnCl_3$ as the electron-transporting layer (n-type). The authors introduced various modifications to the device layers, including adjustments to layer thickness. Specifically, for MASI as the light-absorbing layer, a significant reduction in device efficiency and short-circuit current density (J_{sc}) was observed at thicknesses of 200 nm or greater, which was attributed to charge recombination. From these results, the authors also reduced the thickness of the ETL ($CH_3NH_3SnCl_3$), as it is closer to the surface of the absorber layer and can enhance the conduction of absorbed charges. The highest efficiency was achieved with an ETL thickness of 10 nm, while the MASI layer, used as a p-type layer, was optimized at a thickness of 600 nm. Finally, an efficiency of 16.19% was achieved, considering a high value of N_t (1×10^{17} cm^{-3}) in the light-absorbing layer.

Danladi *et al.* (2022)[65] investigated how the thickness of the MASI and ETL (ZnO) layers affects the overall efficiency of an n–i–p PSC, using CuO as the HTL and a high N_t of 1×10^{16} cm^{-3}. By varying the MASI thickness between 100 and 1000 nm, the highest PCE value was obtained with a 600 nm of perovskite layer. Below this thickness, light absorption was less efficient, as above 600 nm, the efficiency values declined. Regarding ETL, an increase in thickness reduced J_{sc}, and consequently, the PCE values decreased, therefore optimizing its thickness at 300 nm. The authors obtained a final efficiency of 15.10% with the optimizations performed.

2.2 PSCs based on other metals instead of tin

In order to overcome the toxicity caused by lead in PSCs, elements with a +2 oxidation state are possible candidates for

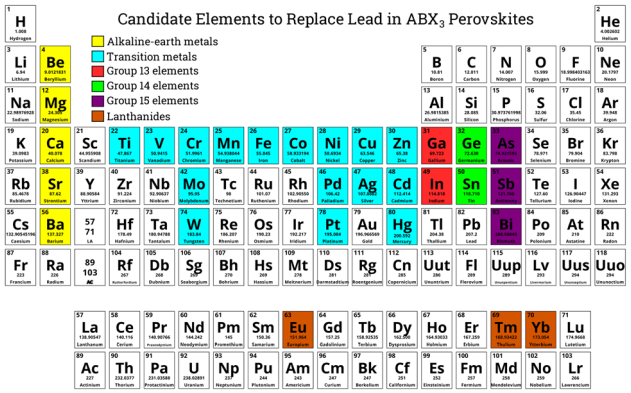

Fig. 11 Elements studied as potential substitutes for lead in ABX_3 perovskites, inspired by Chatterjee and Pal (2018)[36] and Filip and Giustino (2016).[66]

its replacement, as illustrated in Fig. 11. Lead belongs to group 14, and elements from the same group, such as tin and germanium, have similar electronic configurations, which can facilitate substitution.

With regard to germanium, the cation that occupies the A site of Ge-perovskites plays a fundamental role in the performance of these solar cells because when cations such as methylammonium (MA) and formamidine (FA) are used in their structure, the bandgap of the material is very large (or wide), which makes its light absorption not very efficient. Cations even larger than those mentioned affect not only the bandgap but also the dimensionality of the perovskite, thereby worsening the device's performance. Smaller cations, such as cesium, are ideal for Ge-perovskites, as their use maintains the dimensionality of the material, in addition to leading to a smaller bandgap, which is more appropriate for PSCs. Ge-perovskites still face challenges when it comes to oxidation of Ge^{2+}, as is the case with tin.[36,66]

Transition metals and alkaline earth metals are also good alternatives for replacing lead because of their great abundance and low toxicity of most of them. However, while alkaline earth metals can be susceptible to humidity, transition metals commonly used in perovskites generally have smaller ionic radii compared to lead. This reduction in ionic size can decrease the dimensionality of the material. In addition, multiple oxidation states of these metals can affect the chemical stability in perovskite.[36]

Filip and Giustino (2016)[66] investigated, through computational modeling based on DFT calculations, which metals are the best candidates to replace lead at the metallic site. They selected elements with an oxidation state of +2, using Cs as the cation of site A and four different halogens at the X site. Initially, elements with a bandgap below 3.5 eV were chosen. Then, they evaluated which crystal structures preserved the perovskite geometry after structural distortions, and finally analyzed which of these remaining structures exhibited a bandgap smaller than 2 eV. Their study identified perovskites containing Ni and Mg at the metallic site as promising candidates. However, the authors emphasize that none of the metals studied matched the electronic properties of lead, suggesting that mixed Mg–Pb perovskites are a more promising approach than a complete lead replacement.

Group 15 elements, such as antimony and bismuth, have also shown promise as candidates for lead substitution in perovskites. Bi^{-3}, like lead, possesses s-orbital lone pairs and exhibits a high dielectric constant, which can contribute to the detection of defects. Another advantage of bismuth is its lower sensitivity to environmental conditions. It can be used in binary, ternary, or quaternary forms, each presenting specific challenges for practical application: the binary form BiX_3 shows carrier lifetimes insufficient for efficient exciton separation; the films obtained for the ternary form exhibit numerous defects and low luminescence, requiring further investigation of their photophysical properties; finally, in the case of quaternary double perovskites, their wide bandgap limits potential applications, highlighting the need to explore additional structures of this type.[67]

As highlighted by Chen *et al.* (2025),[68] double perovskites are considered a viable option for lead-free materials. However, they face challenges such as the limited tunability of their emission properties, as mentioned above for bismuth. Strategies such as doping can help to tailor the luminescence properties of lead-free perovskites. Antimony, which also possesses lone pair s-orbitals, is an attractive element to enhance these capabilities. The Sb^{3+} ion can introduce additional electronic states that improve optical absorption, thereby increasing light-harvesting efficiency.

Based on this context, the second part of this review focuses on key simulation studies involving perovskites containing metals other than tin at the metallic site, aiming to highlight promising candidates and approaches beyond the traditional lead- and tin-based materials.

2.2.1 Composition and interface engineering in PSCs using other metals instead of tin at the B-site. Chakraborty *et al.* (2019)[69] analyzed four perovskites using cesium as the cation at the A site and titanium as the metal at the B site. Since cesium and titanium perovskites have variable bandgaps, ranging from 1.4 to 1.8 eV, the authors varied the X-site anion to assess the influence of these exchanges. The perovskites studied were Cs_2TiBr_6, Cs_2TiI_6, Cs_2TiF_6 and Cs_2TiCl_6. The n–i–p configuration of the simulated PSC is CuSCN(HTL)/Cs_2TiX_6/CdS(Buffer layer)/p-Si. Initially, the influence of the absorber layer thickness was evaluated, varying it between 100 nm and 4000 nm. The best performance was obtained when the thickness reached 1500 nm for all perovskites, except the Cs_2TiBr_6 perovskite, which achieved the highest PCE among the four PSCs of 6.68%, for a thickness of 1000 nm.

Since the output parameters, J_{sc} and V_{oc}, are highly sensitive to the device temperature, the study evaluated this influence considering temperatures ranging from 27 to 100 °C. For the perovskites Cs_2TiBr_6, Cs_2TiF_6 and Cs_2TiCl_6, J_{sc} increased with increasing temperature, attributed to the reduction in the material's bandgap, which led to the generation of more electron–hole pairs. In contrast, V_{oc} decreased as the temperature increased due to the increase in the saturation current (J_0). In contrast to this behavior, the perovskite Cs_2TiCl_6 exhibited a nearly constant V_{oc}, while J_{sc} still increased with temperature.

The optimized operating temperatures were identified as 80 °C for the bromine-based perovskite, 60 °C for the iodine-based one, and 75 °C for both the chlorine and fluorine-based perovskites. The authors also investigated how variations in series resistance, which primarily affect parameters such as FF and J_{sc}, influence device performance.

The authors did not report the defect density values assumed for the perovskite layers under investigation. Instead, it briefly mentioned bulk recombination of carriers as a possible reason for the limited improvements in J_{sc}, V_{oc}, and PCE with increased absorber thickness. Without explicit N_t data, the discussion loses robustness, since defect density is an essential parameter to produce predictions that more accurately reflect real device behavior.

Hussain *et al.* (2021)[70] simulated a PSC using double perovskite $(FA)_2BiCuI_6$ as the absorber layer, where two formamidinium (FA) cations occupy the A site, replacing the methylammonium (MA) cation, and bismuth and copper replace lead at the B site, in order to address problems such as instability and toxicity. The studied solar cell had the TiO_2/$(FA)_2BiCuI_6$/Spiro-MeOTAD structure in the regular configuration. The authors first compared the output parameters of the PSC using the double perovskite with those of a standard PSC based on MAPI as the absorber layer. The efficiency of the $(FA)_2BiCuI_6$, based PSC was 24.98%, while the MAPI-based solar cell reached 26.43%, considering an N_t of 2×10^{13} cm^{-3} in the $(FA)_2BiCuI_6$ layer. Experimental data from the literature corroborate the simulation results, highlighting the potential of $(FA)_2BiCuI_6$ as a promising lead-free alternative for PSCs.

The study evaluated the influence of interface defects on device performance by analyzing two interface defect layers: IL1, located between TiO_2 (ETL) and $(FA)_2BiCuI_6$, and IL2, located between Spiro-MeOTAD (HTL) and $(FA)_2BiCuI_6$. The N_t values were varied from 10^{13} to 10^{17} cm^{-3} for IL1, and from 10^{13} to 10^{21} cm^{-3} for IL2. The results showed that lower N_t values at both interfaces led to higher efficiency and improved output parameters.

Finally, the authors also evaluated the influence of variations in the charge carrier mobility in the absorber layer, considering values ranging from 2×10^{-3} to 20 cm^2 V^{-1} s^{-1}. Fig. 12 shows that V_{oc} decreases when charge mobility increases, while J_{sc} increases with increasing electron mobility (μ_e). This occurs because, with high charge carrier mobility, the carrier density in the depletion region decreases, reducing the V_{oc}. In contrast, a decrease in the mobility of the charge carrier negatively affects J_{sc}, as the probability of dissociation and recombination of the charge increases, reducing both FF and PCE. Therefore, a value of 2 cm^2 V^{-1} s^{-1} was observed to be optimal to balance the output parameters.

In the work of Ashfaq *et al.* (2023),[71] the use of single, double or triple layers of the perovskite Cs_2TiX_6, with X being one of the halides Br^-, Cl^- or I^-, was evaluated as the absorber layer in a PSC, using IGZO as ETL and $CuSbS_2$ as HTL in a PSC with n–i–p configuration. Although the authors adopted an N_t of 10^{10} cm^{-3}, claimed as the fabrication limit for lead-free perovskites, this value is unrealistically low even compared to typical Pb-based PSCs, as previously discussed in this review. Consequently, the resulting device performances are overly optimistic

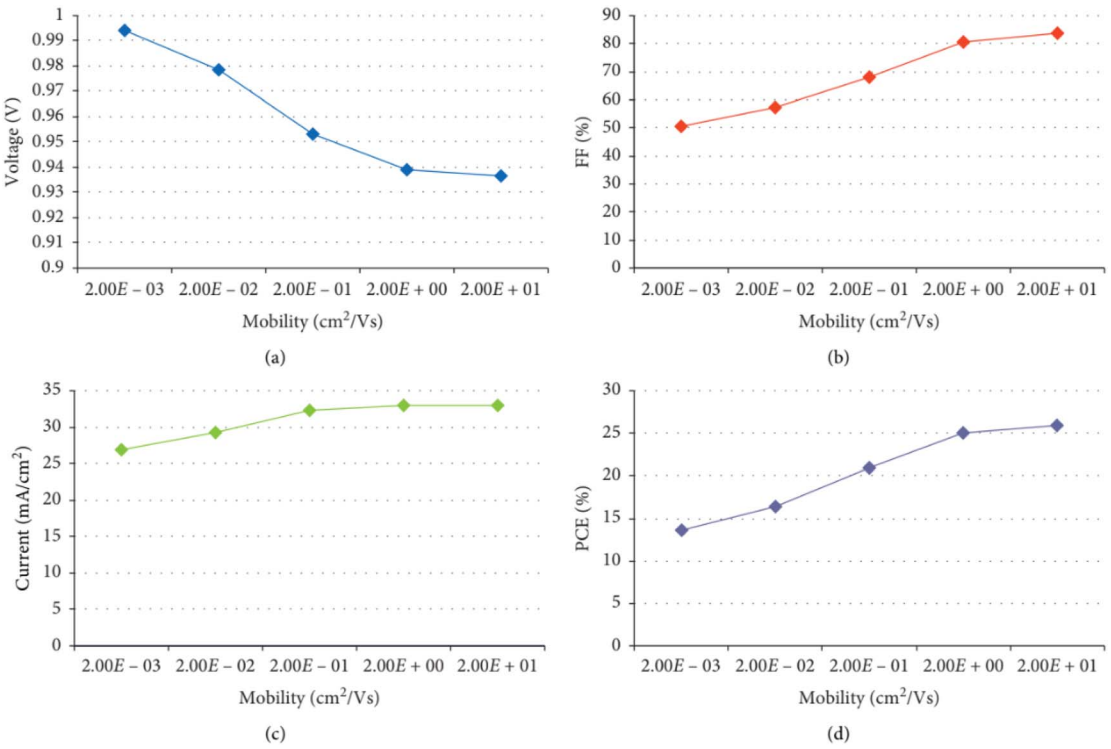

Fig. 12 Variation of V_{oc} (a), FF (b), J_{sc} (c) and PCE (d) according to charge mobility, reproduced from Hussain *et al.* (2021)[70] (https://doi.org/10.1155/2021/6668687) under the Creative Commons Attribution License.

and do not reflect experimental realities, thereby limiting the practical relevance of the simulations. In particular, the study showed that the values for J_{sc}, V_{oc}, FF and PCE did not differ significantly between N_t values ranging from 10^{10} to 10^{13} cm^{-3}, raising questions about the practical relevance of assuming extremely low N_t values.

After optimization, single-layer solar cells using Cs_2TiBr_6 and Cs_2TiI_6 perovskites achieved the best results, including efficiencies of 29.19% and 22.56%, respectively. The PSC with the Cs_2TiCl_6 absorber layer achieved an efficiency of only 12.68%. The PSC using the double layer of Cs_2TiBr_6/Cs_2TiCl_6 perovskites achieved a slightly higher PCE than that of the single layer using the bromine-containing perovskite composition of 30.06%. The simulated solar cell with the triple absorber layer achieved an efficiency of only 13.19%.

Kundara and Baghel (2023)[72] simulated n–i–p PSCs with copper-based perovskites, $(MA)_2CuCl_4$, $(MA)_2CuCl_2I_2$, and $(MA)_2CuCl_2Br_2$, using an ideal N_t value of 10^{13} cm^{-3}. Different ETLs (PCBM, C_{60}, TiO_2) and HTLs (PEDOT:PSS, Cu_2O, CuI, Spiro-MeOTAD) were evaluated, with subsequent optimization of perovskite thickness. The best configurations achieved PCEs of 18.41%, 17.38%, and 28.31% for $(MA)_2CuCl_4$, $(MA)_2CuCl_2I_2$, and $(MA)_2CuCl_2Br_2$, respectively. Compared with experimental reports, which produced PCEs below 3% for all three absorbers, the significantly lower experimental efficiencies were attributed to the use of TiO_2 and Spiro-MeOTAD as charge transport layers, considered unsuitable for these compositions.

Hasan *et al.* (2024)[73] investigated the use of zincoxy-sulfide ETL ($ZnO_{0.25}S_{0.75}$) in a PSC with n–i–p configuration, using antimony-containing perovskite in the metal site, $Cs_3Sb_2I_9$, as the absorber layer, and Spiro-MeOTAD as the HTL. The authors note that the experimental efficiencies obtained for antimony perovskites remain very low (1.8–2.5%) due to charge recombination losses and inadequate band alignment at the PSC interfaces. The composition engineering performed in the ETL was chosen as the method because the previous simulation study carried out by Zhang *et al.* (2023),[74] cited in this review, demonstrated the potential of this approach in the ETL. The optimized PSC has the Mo/Spiro-MeOTAD/$Cs_3Sb_2I_9$/$ZnO_{0.25}S_{0.75}$/FTO/Al configuration. In this work, the defect density attributed to perovskite was considered ideal (10^{14} cm^{-3}). After studying the influence of the thicknesses of the active layers and changes in the defects value at the interfaces, an efficiency of 20.25% was reached, a value much higher than in the experimental studies.

Noman *et al.* (2024)[75] investigated the use of a BiI_3 layer at the interface between the perovskite and the HTL, in order to passivate defects and improve hole extraction, employing Spiro-MeOTAD and TiO_2 as HTL and ETL, respectively. For comparison, both the lead-free perovskite $MAGeI_3$ and the Pb-based perovskite $MAPbI_3$ were used, with both PSCs configured in the regular architecture. An ideal defect density (N_t) of 1×10^{14} cm^{-3} was assumed in the $MAGeI_3$ layer.

When comparing the energy band alignment of the lead-free perovskite and the HTL with and without the BiI_3 interlayer (Fig. 13), the authors observed that the presence of the BiI_3 layer had a more significant effect on the $MAGeI_3$ perovskite than on the MAPI-based PSC.

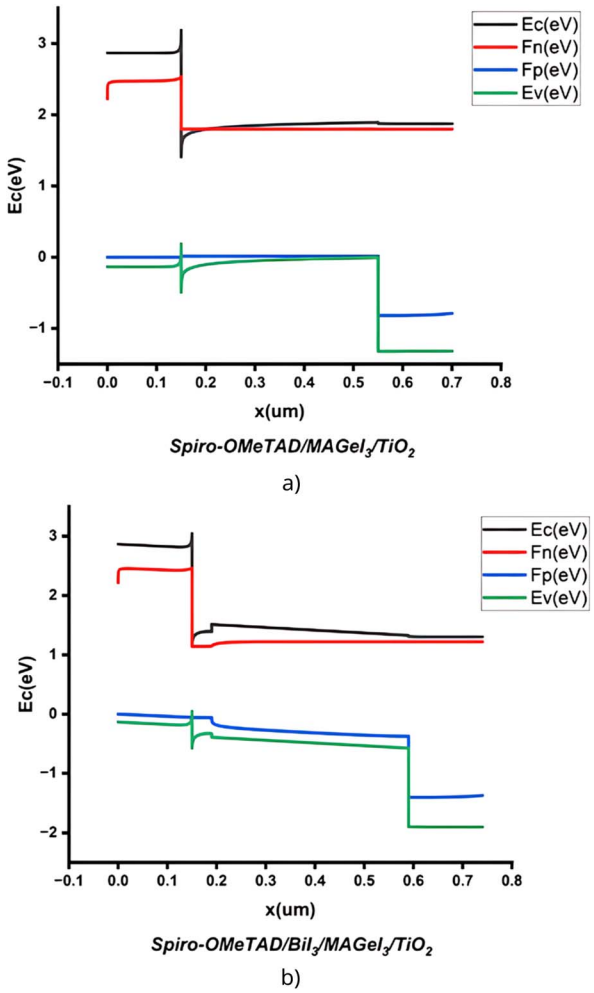

Fig. 13 Energy band alignment of the $MAGeI_3$ perovskite/HTL interface: (a) without and (b) with the BiI_3 interlayer. Reproduced and adapted from Noman *et al.* (2024)[75] (doi: https://doi.org/10.1038/s41598-024-56246-4) under a Creative Commons Attribution (CC BY 4.0) license.

The formation of a cliff can be observed at the perovskite/HTL interface in graph (a) (Fig. 13), with a valence band offset (VBO) of −0.68 eV. This cliff causes a substantial hole-blocking barrier at the interface, negatively impacting solar cell efficiency. With the addition of the interlayer, hole transport is facilitated, with the VBO between $MAGeI_3$ and BiI_3 reaching −0.06 eV, significantly reducing the cliff between the interfaces while still maintaining a slight offset that helps suppress charge recombination. With the use of the interlayer, the PSC efficiency increased from 11.90% to 15.57%.

Abbasi *et al.* (2025)[76] proposed a PSC using $CsInCl_2$ as the absorber layer. Indium was selected for its lower toxicity and higher oxidation resistance compared to lead, while cesium was chosen for the A-site due to its thermal stability. Chlorine was used as the X-site halide because its stronger ionic bonding, relative to iodine, reduces halide migration in the crystalline

film. Despite these advantages, $CsInCl_3$ demonstrated poor performance compared to MAPI, mainly due to suboptimal light absorption and inefficient charge carrier dynamics. One strategy that can be used to overcome this limitation is the plasmonics effect, which is based on the interaction of light with free electrons from metal nanoparticles, such as silver (Ag) and gold (Au). The authors report that this is the first study to investigate the use of Au and Ag dopants at the indium metal site through DFT calculations and SCAPS-1D simulations.

The regular device used *N*,*N*′-bis-(1-naphthalenyl)-*N*,*N*′-bis-phenyl-(1,1′-biphenyl)-4,4′-diamine (nPB) as the HTL and Alq_3 ($Al(C_9H_6NO)_3$) as the ETL, with an ideal N_t value of 1×10^{14} cm^{-3} in the perovskite layer. From the computational calculations, the perovskites $CsInCl_3$, Ag-doped $CsInCl_3$, and Au-doped $CsInCl_3$ exhibited bandgaps of 1.632 eV, 1.404 eV, and 1.101 eV, respectively. Based on these results and on the CBO and VBO values calculated from SCAPS-1D simulations, it was observed that the device with Au-doped $CsInCl_3$ presented a nearly ideal band alignment and, consequently, a high PCE (25.53%) compared to the PSC with Ag-doped $CsInCl_3$ (20.57%) and the PSC with pure $CsInCl_3$ (17.66%).

2.2.2 Influence of ETLs/HTLs in PSCs using other metals instead of tin at the B-site. Lakhdar and Hima (2020)[77] analyzed the effect of ETL when $CH_3NH_3GeI_3$ perovskite was used as the absorber layer in a PSC with a p–i–n configuration. The authors also simulated PSCs using MAPI for comparison and initial validation purposes. Different ETLs (PCBM, IGZO, SnO_2, fullerene-C_{60}, ZnO and TiO_2) were used in the simulations, and it was observed that using thickness values of 50 nm for the ETL and 650 nm for the perovskite layer with an N_t considered ideal, the best efficiencies were achieved when C_{60}, SnO_2 and TiO_2 were used. The lowest PCE was observed for the PSC using IGZO, which the authors attributed to the band misalignment between this ETL and the perovskite.

Ahmed *et al.* (2021)[78] proposed an all-inorganic n–i–p PSC using Cs_2TiBr_6 as the absorber layer, investigating different ETL and HTL materials. The N_t value is 4.17×10^{15} cm^{-3} in the perovskite layer. As HTLs, the candidates evaluated were CuSCN, CuI, NiO, and MoO_3. The VBO was calculated for each HTL, and all showed negative values, indicating the absence of a barrier for hole transport from the perovskite to the electrode. Among them, MoO_3 exhibited the best band alignment with the inorganic perovskite, resulting in a simulated PCE of 4.58%. For the ETLs considered in the simulations (SnO_2, ZnO, TiO_2, and CdS), SnO_2 provided the best performance, with a PCE of 4.75% using an absorber thickness of 130 nm. After further optimizations, including adjustments to the thickness of the HTL and ETL layers, as well as reductions in the defect density of both the perovskite and the interfaces, the device configured as FTO/SnO_2/Cs_2TiBr_6/MoO_3/Au achieved a PCE of 11.49%.

He *et al.* (2021)[79] performed the first simulation study applying $Cs_4CuSb_2Cl_{12}$ perovskite (CCSC) as an absorber layer in a PSC. The authors chose this material for its photoelectric properties, demonstrated in previous studies, suitable bandgap for PSCs (around 1.0 eV), and environmental stability. However, CCSC has low charge mobility, which can impact its performance as an absorber layer. Experimentally, this limitation can be mitigated through the use of CCSC nanocrystals. Consequently, different ETLs and HTLs were evaluated in an n–i–p solar cell configuration, using an N_t in the CCSC of 1×10^{15} cm^{-3}.

The authors analyzed the use of P3HT, PEDOT:PSS, Cu_2O, CuI, and Spiro-MeOTAD as HTLs, while keeping TiO_2 as the ETL in the simulations. Among them, Cu_2O was the only HTL that presented a positive VBO. A large positive VBO at the HTL/absorber interface can form an energy spike that hinders hole transport. A small VBO at the HTL/absorber interface not only avoids significant barriers to hole extraction but also increases the activation energy, contributing to reduced charge recombination. This effect was confirmed in the simulations, as the best device performance was achieved with Cu_2O as the HTL, reaching a PCE of 16.11%. With Cu_2O fixed as the HTL, the influence of different ETLs, TiO_2, PCBM, ZnO, and IGZO, was evaluated. All configurations exhibited negative CBO values. The ETL TiO_2 provided a slightly higher PCE (16.11%) compared to PCBM (16.01%), mainly attributed to its higher dielectric constant. After further optimizations, including adjustment of layer thicknesses and interface defect densities, the device achieved a maximum efficiency of 23.07%.

Deepthi Jayan and Sebastian (2021)[80] conducted a study to compare the performance of a lead-free PSC using $MAGeI_3$ perovskite with a Pb-based PSC using MAPI in a regular configuration. Different materials were used as ETLs, HTLs, and metallic contacts. The N_t used in the study was considered ideal for both perovskites. Better performance was achieved for both PSCs when inorganic ETLs and HTLs replaced organic materials. Thus, the optimized configurations with the best output parameters were for the lead-containing solar cell FTO/SnO_2/$MAPbI_3$/NiO/Au, obtaining 20.80% efficiency and for the lead-free PSC, FTO/SnO_2/$MAGeI_3$/CuO/Pd with a PCE of 13.12%. From the Quantum Efficiency (QE) graph of the PSCs, it was observed that the solar cell using $MAGeI_3$ reaches a QE of zero at 660 nm, while the Pb-based PSC does so at 830 nm. This difference is attributed to the larger bandgap of the lead-free PSC (1.9 eV), which results in reduced absorption of photons in the near-infrared region. Consequently, this is one of the factors that contributes to the lower efficiency of the lead-free solar cell.

Ahmad *et al.* (2022)[81] employed different ETLs (WS_2, ZnO, SnO_2, TiO_2, ZnSe, and WO_3) in simulations using the perovskite $NH_3(CH_2)_2NH_3MnCl_4$ as the light-absorbing layer in a solar cell with n–i–p configuration. Defect density was set at 10^{15} cm^{-3} in the perovskite layer. The simulated device with ZnSe as the ETL demonstrated slightly higher efficiency (20.30%) compared to the other ETLs. This improvement was attributed to the high electron and hole mobility of ZnSe, together with favorable energy level alignment with the perovskite, which facilitated electron transport. The authors also fabricated a PSC using the perovskite $NH_3(CH_2)_2NH_3MnCl_4$ and TiO_2 as an ETL to validate the simulated results. The experimental device exhibited an efficiency of only 0.12%, which the authors attributed to defects in the perovskite film and its rapid crystallization.

Chabri *et al.* (2022)[82] performed several simulations by changing the ETL (SnO_2, ZnO and CdS) and HTL (CuI, NiO and

MoO_3) of an n–i–p PSCs using the all-inorganic perovskite Cs_2TiI_6. After selecting MoO_3 and ZnO as HTL and ETL materials, respectively, the authors optimized the thicknesses of the transport and absorber layers, also varying the defect density values of the inorganic perovskite between 10^{11} and 10^{16} cm^{-3}. At the end of the optimizations, they obtained an efficiency of 22.50%, using an N_t of 10^{12} cm^{-3}. It is worth noting that, as in other studies discussed in this review, a defect density below the commonly accepted ideal value was used, potentially leading to unrealistic simulated device results.

Pindolia *et al.* (2022)[83] tested different inorganic ETLs and HTLs in n–i–p PSCs incorporating the perovskite $RbGeI_3$, using an N_t of 10^{15} cm^{-3}. In the case of HTLs, when TiO_2 was used as ETL, CuI delivered the highest PCE (12.81%) among the tested materials. However, the FF value presented by the device was very low, at only 12.21%. Based on these results, NiO was selected as the HTL for further optimizations, achieving an efficiency of 9.89% and a FF of 64.28% when used in the solar cell, with a thickness of 100 nm. Regarding the ETLs, WS_2 showed inferior performance, mainly due to its low bandgap and highly negative CBO. In contrast, TiO_2 provided the best results. Following additional optimizations, the PSC with the FTO/TiO_2/$RbGeI_3$/NiO/Ag configuration reached an efficiency of 10.11%.

Jan and Noman (2022)[84] simulated a PSC in the regular n–i–p configuration, using the lead-free perovskite containing germanium in the metallic site and methylammonium in the cationic site, $MAGeI_3$, and TiO_2 as ETL. Considering an N_t of 10^{14} cm^{-3}, a significant increase in solar cell efficiency was observed when copper HTLs replaced Spiro-MeOTAD. The use of $CuSbS_2$ increased PCE from 17.74% to 21.42%, while the $CuAlO_2$ HTL achieved an efficiency of 23.56%.

Ahmad *et al.* (2023)[85] simulated four different inverted PSC architectures using $CsGeI_3$ as the absorber layer, selected as a fully inorganic and less toxic alternative to lead-based perovskites. Moreover, $CsGeI_3$ has a bandgap of 1.65 eV, which is closer to that of $MAPbI_3$ (1.55 eV) compared to the germanium-based $MAGeI_3$ (1.9 eV). The defect density in the perovskite was set to 1×10^{14} cm^{-3}. The simulated configurations were C_{60}/$CsGeI_3$/CuSCN; C_{60}/$CsGeI_3$/$CuSbS_2$; PCBM/$CsGeI_3$/CuSCN; and PCBM/$CsGeI_3$/$CuSbS_2$. Devices employing C_{60} as the ETL outperformed those using PCBM, with the FTO/C_{60}/$CsGeI_3$/CuSCN/Au configuration achieving the highest efficiency of 12.24%.

For an ideal band alignment between the ETL and the perovskite, a minimal CBO and a maximal VBO are required to ensure a continuous electron flow while blocking hole transport. For C_{60} and PCBM, the CBO values with the $CsGeI_3$ perovskite are identical because of their similar electron affinities. However, the VBO values differ: PCBM exhibits a VBO of 0.8 eV, higher than C_{60} (0.5 eV), which is attributed to its larger bandgap. Given this similarity in CBO, the authors attributed the differences in output parameters to the HTLs. The use of $CuSbS_2$ induces small offsets in both the conduction and valence bands, creating pronounced spikes at the perovskite/HTL and ETL/perovskite interfaces. These spikes promote carrier trapping, increase recombination, and reduce PCE in devices with both C_{60} and PCBM, compared to those using CuSCN as the HTL. These spikes can be observed in Fig. 14 for PSCs with C_{60} (a) and PCBM (b), where the green line represents the valence band energy (E_v) and the black line the conduction band energy (E_c). However, although the authors attribute the performance variation exclusively to the HTLs, it is evident that changing the ETL also significantly affects the output parameters. For instance, V_{oc} increased from 0.69 V in the PCBM/$CsGeI_3$/CuSCN PSC to 0.88 V in the C_{60}/$CsGeI_3$/CuSCN cell. Further optimizations were carried out, including adjustments in layer thicknesses and defect densities. As a result, the best performance was achieved with the C_{60}/$CsGeI_3$/CuSCN PSC, reaching a V_{oc} of 1.0169 V, a J_{sc} of 19.653 mA cm^{-2}, an FF of 88.13%, and an optimized PCE of 17.61%.

Hossain *et al.* (2023)[86] investigated the potential of bismuth-based perovskite $Cs_3Bi_2I_9$ as a light-absorbing layer in a regular PSC, using DFT calculations and evaluated different HTLs and ETLs for this material through SCAPS-1D simulations. DFT

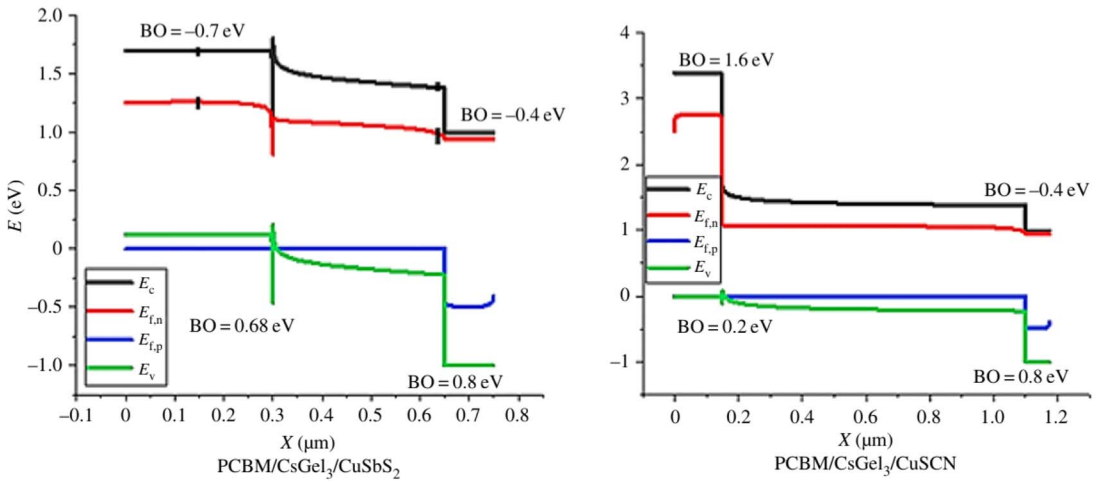

Fig. 14 Energy band alignments of PSCs using PCBM as the ETL and CuSCN and $CuSbS_2$ as HTLs. Reproduced by Ahmad *et al.* (2023)[85] (https://doi.org/10.1098/rsos.221127) under a Creative Commons Attribution (CC BY 4.0) license.

calculations were used to determine parameters related to the structural properties of $Cs_3Bi_2I_9$ perovskite, such as the band structure, the density of states and defects and the optical properties. Subsequently, the simulation study was carried out using SCAPS-1D, and the best performance (with an efficiency of 16.61%) was achieved when WS_2 was used as the ETL and Cu_2O as the HTL in the regular PSC with the configuration ITO/WS_2/$Cs_3Bi_2I_9$/Cu_2O/Au, considering an N_t of 10^{15} cm^{-3} in the absorber layer.

Zhang *et al.* (2023)[74] investigated the use of different hole and electron transport layers (HTLs and ETLs) for devices based on $Cs_3Sb_2I_9$ antimony perovskite. Although solar cells employing this perovskite still exhibit low efficiency in experimental devices, they based their simulations on previously reported properties, including the higher stability of $Cs_3Sb_2I_9$ films compared to MAPI when fabricated *via* the two-step deposition method,[87] along with a suitable bandgap of 2 eV.[88] Based on these conclusions, the authors carried out simulations using SCAPS-1D combined with DFT calculations to evaluate how the band alignment of different materials with the perovskite can improve PSC performance in the n–i–p configuration, considering an ideal defect density (N_t) for $Cs_3Sb_2I_9$.

Among the ETLs analyzed, ZnOS exhibited significantly superior performance compared to the others. While the devices using WS_2, CdS, TiO_2, SnO_2, and ZnO reached PCE values of 2.00%, 3.23%, 4.34%, 5.47%, and 4.52%, respectively, the solar cell with ZnOS achieved a much higher efficiency of 12.34%. This outstanding result is directly attributed to its favorable CBO of −0.3 eV, which enables efficient electron extraction while minimizing recombination losses. In addition to the highest PCE, the device with ZnOS also showed superior values for all other output parameters, including the FF, confirming that this ETL offers the best energy level alignment with the $Cs_3Sb_2I_9$ perovskite among those evaluated.

Regarding the different HTLs studied, the one that presented the best performance was Cu_2O, achieving an efficiency of 13.86%. After further optimizations, including adjustments in the layer thickness and the type of metal contact used, the authors determined that the FTO/ZnOS/$Cs_3Sb_2I_9$/Cu_2O/C configuration yielded the best performance, achieving a final efficiency of 18.29%.

Mehrabian *et al.* (2023)[89] investigated the influence of different ETLs (ZnO, C_{60}, CdS, SnO_2, PCBM, and TiO_2) on the performance of a regular PSC, using the double perovskite $Cs_2AgBiBr_6$ as the absorber layer, which contains aluminum and bismuth as B-site metals. The inorganic HTL selected for the study was Cu_2O. Initially, considering an absorber thickness of 50 nm, the highest efficiency (18.40%) was obtained with ZnO as the ETL, while the lowest (12.11%) occurred using SnO_2, mainly due to the band misalignment between SnO_2 and $Cs_2AgBiBr_6$ perovskite. When the thickness of the absorber layer was increased to 400 nm, the PCE with ZnO further improved, reaching 20.08%, assuming a defect density (N_t) of 10^{14} cm^{-3}.

Rehman *et al.* (2024)[90] also investigated the influence of different HTLs, ETLs, and other parameters on the performance of a PSC using potassium germanium trichloride ($KGeCl_3$) perovskite as the absorber layer. The authors emphasize that incorporating cations such as potassium (K) and rubidium (Rb) in the A-site of the perovskite, instead of organic compounds like MA and FA, improves the thermal stability of the PSC. For this perovskite, WS_2 demonstrated good performance as the ETL, combined with MoO_3 as the HTL. Assuming an ideal defect density (N_t) of 10^{13} cm^{-3}, the device with a p–i–n configuration of FTO/MoO_3/$KGeCl_3$/WS_2/Au achieved a FF of 81.76% and a PCE of 29.83%.

Utsho *et al.*(2025)[91] investigated the impact of different ETLs (WS_2, C_{60}, PCBM and TiO_2) on the performance of an n–i–p PSC using double perovskite $Cs_2CuBiBr_6$ as the absorber layer and Cu_2BaSnS_4 (CBTS) as HTL. The study also explored the influence of varying the thicknesses of both the absorber and ETL layers. Among the configurations, the best performance was achieved with a perovskite thickness between 500 and 650 nm and a WS_2 ETL thickness between 30 and 150 nm, reaching a PCE of 19.71%, the highest of all simulated devices, using an N_t of 1×10^{15} cm^{-3} in the absorber layer. The superior performance of WS_2 is attributed to its ideal CBO of zero with the perovskite, which enables efficient electron transport without introducing energy barriers. After further optimizations, the device with the ITO/WS_2/$Cs_2CuBiBr_6$/CBTS/Ni configuration delivered the best overall performance, mainly due to the favorable band alignment between the layers.

Kundara and Baghel (2025)[92] investigated the use of different ETLs (CdS, PCBM, C_{60}, WS_2) and HTLs (CuI, Spiro-MeOTAD, Cu_2O, PEDOT:PSS, MoS_2) in a PSC in the inverted configuration using the perovskite $KGeCl_3$ and an N_t of the absorber layer considered ideal (1×10^{13} cm^{-3}). Among the different configurations tested, the one that obtained the highest efficiency (25.61%) was FTO/WS_2/$KGeCl_3$/PEDOT:PSS/Au. Subsequently, the authors performed further optimizations involving variable parameters, such as absorber thickness and donor and acceptor carrier concentration values (N_D and N_A) values, achieving a PCE of 31.00%.

Shimul *et al.* (2025)[93] analyzed the use of WS_2, ZnO, PCBM, and C_{60} as ETLs in an n–i–p PSC employing Cu_2O as the HTL and a magnesium arsenic perovskite (Mg_3AsBr_3) as the absorber layer. The application of this type of perovskite has been increasingly investigated for photovoltaic purposes through computational modeling. Accordingly, the study employed DFT calculations to determine optoelectronic properties such as the band structure and density of states (DOS). Subsequently, the authors used the SCAPS-1D and wxAMPS simulation tools to evaluate the device performance using this absorber layer, assuming an ideal defect density (1×10^{14} cm^{-3}). After various optimizations, the results obtained from the two simulation software packages were highly consistent, with the device using WS_2 as the ETL exhibiting the best performance (32.55%) and the PSC with C_{60} as the ETL showing the lowest efficiency (31.63%).

Ijam (2025)[94] explored the application of different ETLs [IGZN, PCBM, TiO_2, WS_2, and $Zn(O_{0.3},S_{0.7})$] and HTLs [graphene oxide (GO), MoO_3, Sb_2S_3, V_2O_5, Zn_3P_2, and $CuSbS_2$] in a regular PSC using the double perovskite $Cs_2AgBi_{0.75}Sb_{0.25}Br$, as the light-absorbing layer. An ideal defect density ($N_t = 1 \times 10^{14}$ cm^{-3}) was assumed for the absorber. When Zn_3P_2 was fixed as

the HTL, the device simulated with $Zn(O_{0.3}, S_{0.7})$ as the ETL showed the best output parameters, reaching a PCE of 17.57%. Keeping this ETL and varying the HTLs, V_2O_5 yielded the highest values of J_{sc}, FF, and PCE, achieving an efficiency of 21.05%. This superior performance was attributed to its VBO of +0.22 eV, which resulted in a spike at the HTL/absorber interface. In contrast, the worst performance was obtained with GO as the HTL, resulting in a PCE of only 12.20%, which was correlated with a VBO of −0.6 eV, forming a cliff at the HTL/absorber interface. After optimizing the thicknesses of the absorber layer and the transport layers (ETL and HTL), the study reported a maximum PCE of 28.43% and a FF of 91.94% for the device configured as $FTO/Zn(O_{0.3}, S_{0.7})/Cs_2AgBi_{0.75}Sb_{0.25}Br/V_2O_5/Pt$.

2.2.3 Influence of adjustable parameters on PSC performance (doping concentration and defect density) in PSCs using other metals instead of tin at the B-site. Miah *et al.* (2023)[95] modified various factors, including the thickness of the solar cell layer, the defect density, the temperature and resistance, to optimize the all-inorganic $TiO_2/CsGeI_3/MoO_3$ PSC in an n–i–p configuration. $CsGeI_3$ perovskite was chosen based on promising results obtained from the experimental studies. MoO_3 oxide was chosen as the HTL due to several factors, including its good environmental stability and the ability to form an interface that fits both the absorber layer and the rear contact electrode. Finally, TiO_2 was chosen as ETL due to its thermal and chemical stability.

The authors varied the bulk and amphoteric defect density of the perovskite between 1×10^{10} and 1×10^{17} cm^{-3}, observing a significant decrease in the values of the output parameters, especially the FF and the PCE. The authors optimized the bulk and amphoteric defect density at 1×10^{12} cm^{-3}. As in other studies analyzed in this review, an N_t below the ideal was used, once again rendering the efficiency (22.84%) and other output parameters achieved in this work unrealistic. The increase of the interface defect density from 1×10^{11} to 1×10^{15} cm^{-2} affected the ETL/$CsGeI_3$ interface more significantly than the $CsGeI_3$/HTL interface.

Different metals were tested as rear contacts, with varying work function values. The best performance was achieved when metals with a work function between 5.0 and 5.7 eV were used. This result aligns with the literature, as metals with higher work function values have their Fermi level closer to the valence band, which facilitates the transport of majority carriers. In PSCs with a regular configuration, this majority carrier is typically the hole, since the metal electrode is directly in contact with the HTL. Finally, after further optimizations, including temperature variations and series resistance adjustments, the authors achieved a PCE of 22.85% for the studied PSC.

Mahammedi *et al.* (2024)[96] optimized several parameters to enhance the performance of a PSC based on the double perovskite Bi_2FeCrO_6 (BFCO), which contains iron and chromium at the B-site. This perovskite is a multiferroic material, allowing for tunable bandgap properties. The authors used two experimental PSCs as reference points to validate their initial simulations and to investigate strategies for enhancing the performance of devices with BFCO as the absorber layer. In both experimental PSCs, niobium-doped strontium titanate ($Nb:SrTiO_3$ or NSTO) was used as the ETL, as this substrate supports favorable growth of the perovskite film due to its compatible crystal structure, thereby reducing the formation of defects in the film.

One of the experimental PSCs was HTL-free, reaching an efficiency of 0.8%, while the other was a p–i–n device using NiO as the HTL and achieved a PCE of 2.0%. Following this initial stage, an n–i–p PSC was simulated with the configuration ITO/n-NSTO/i-BFCO/p-NiO, using the same HTL and ETL as in the experimental p–i–n cell. The simulated solar cell in a regular configuration achieved a slightly higher efficiency of 2.98%, which was attributed to the improved band alignment between the HTL and the perovskite when the device architecture was reversed to n–i–p, as shown in Fig. 15. In the p–i–n configuration, a conduction band spike is observed at the interface between NiO and the perovskite. When this misalignment is too large, it can act as a barrier for electrons, leading to their accumulation at the interface, which promotes interfacial recombination, as indicated by the black curve in the Fig. 15. This charge recombination reduces the output parameters of the device. Subsequently, the authors performed further optimizations regarding layer thicknesses and defect density values. For an N_t of 2×10^{16} cm^{-3} and a BFCO thickness of 150 nm, a PCE of 7.3% was achieved, demonstrating that proper band alignment and optimized thicknesses can significantly enhance the overall device performance.

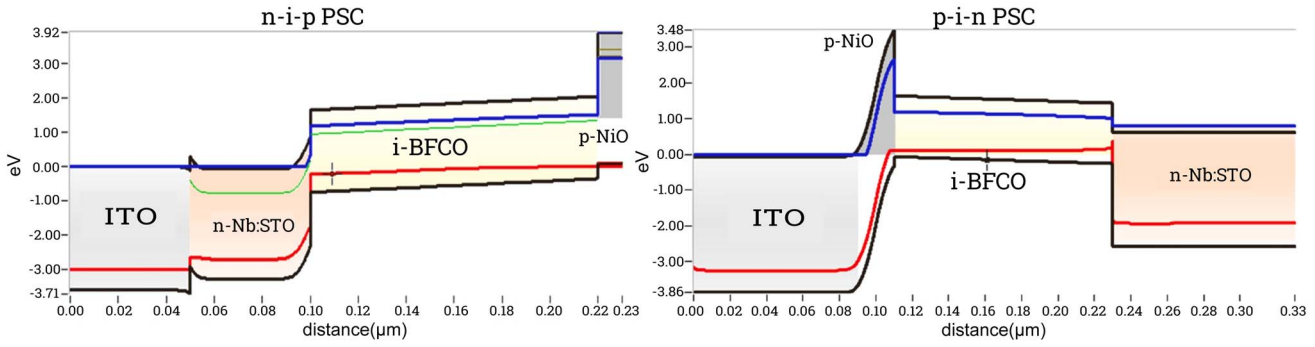

Fig. 15 Band alignment of simulated n–i–p and p–i–n PSCs, reproduced and adapted from Mahammedi *et al.* (2024)[96] (https://doi.org/10.1016/j.ijleo.2024.171659) under a Creative Commons Attribution (CC BY 4.0) license.

Rahaman *et al.* (2024)[97] simulated three different PSCs in the n–i–p configuration, employing La-doped $BaSnO_3$ as the ETL due to its suitable band alignment and high electron mobility, and $CuSbS_2$ as the HTL, one of the copper-based compounds studied as an alternative to organic HTLs in PSCs. The study aimed to evaluate and compare the performance of devices using three different absorber layers: MAPI, MASI, and Cs_2TiBr_6.

The authors varied the perovskite thickness between 500 and 2500 nm and observed that the highest efficiency was obtained for the PSC using MASI, reaching 26.77% at a thickness of 816 nm, followed by 21.15% for Cs_2TiBr_6 (1026 nm) and 20.96% for MAPI (1237 nm). However, the fill factor of the PSC based on MAPI remained higher. The defect density in the absorber layer was also evaluated in the range of 10^{10} to 10^{13} cm^{-3}, along with the effect of temperature on device performance. The authors concluded that MASI perovskite presents the most significant potential as a lead-free alternative in traditional PSCs. As highlighted multiple times throughout this review, an N_t of 10^{10} cm^{-3} is considerably suboptimal, and even unrealistic in practical contexts. However, its recurrent use in simulation-based research articles reinforces the need for a more rigorous discussion of the criteria adopted to define defect density values.

Through DFT calculations, Ravidas *et al.* (2025)[98] obtained the optoelectronic properties of the $RbGeI_3$ perovskite. They used this results to simulate PSCs with different HTLs and ETLs in a solar cell with the n–i–p configuration. The ETLs studied were TiO_2, PCBM, WS_2, C_{60}, and CdS, and the HTLs were the materials Spiro-MeOTAD, $CuSbS_2$, PEDOT:PSS, P3HT and PTAA. The PSC using PTAA as the HTL and TiO_2 as the ETL achieved slightly higher efficiency among other PSC combinations, and was therefore selected for subsequent optimizations. In the end, the output parameters of the remaining configurations showed minor variations, with the PSC yielding approximately 24% efficiency for an N_t considered ideal.

3 Conclusion

This review presented the main advances in lead-free PSC simulations carried out between 2016 and 2025 using the free SCAPS-1D software. Theoretical studies are essential to understand the factors that influence the performance of these devices, allowing the evaluation of parameters such as band alignment, as well as VBO and CBO values. These analyses provide important information for selecting materials that can lead to more efficient and stable solar cells.

A total of 26 studies on lead-free PSCs using tin (Sn) as an alternative B-site metal were analyzed. Among these, 19 investigated devices with the regular n–i–p configuration, while only two employed the inverted architecture. One of the 26 studies, conducted previously by our research group, explored the use of fullerene C_{60} and its derivative PCBM as interlayers in both configurations. Moreover, four studies focused on HTL-free PSCs.

We also discussed results from 28 studies that investigated lead-free perovskites containing alternative B-site metals. Among these studies, single B-site metals such as titanium, germanium, copper, antimony, bismuth, arsenic, manganese, and indium were considered, as well as double perovskites including FeCr, AgBi, CuSb, CuBi, and BiSb. Of these, 23 used the regular configuration, while four adopted the inverted (p–i–n) structure. Only one study explored both architectures and also simulated an HTL-free device.

In general, there is a clear preference for the regular n–i–p configuration in the 54 simulation studies of lead-free PSCs analyzed in this review. This trend contrasts with that observed in lead-based PSCs, where inverted devices (p–i–n) are more frequently adopted due to their better performance in experimental solar cells, particularly in terms of lower hysteresis and compatibility with low-temperature fabrication.[99]

One possible reason for this difference is that the regular structure is more widely established and may be considered a safer and more reliable starting point for lead-free devices, which are still in the process of active development. However, this trend has been changing in recent years, with researchers increasingly preferring to develop lead-free PSCs in the inverted configuration, as highlighted by Aktas *et al.* (2022).[34] As shown in Table 1 of this review, the highest efficiencies of tin-based solar cells reported to date have been obtained in the p–i–n configuration.

The reviewed studies demonstrate that the parameters used in the simulations are critical in ensuring results that closely reflect experimental observations. In particular, the defect density in the absorber layer (N_t) and at the interfaces has a significant impact on the accuracy of the predictions. Assuming idealized N_t values that are substantially lower than those typically found in real devices can lead to overly optimistic and practically unattainable results. Among the studies discussed in this review, 28 employed an N_t value considered ideal (between 10^{13} and 10^{14} cm^{-3}), while 4 used an N_t value below 10^{13} cm^{-3}, which compromises the validity of their results. These four studies that employed sub-ideal N_t values (10^{10}–10^{12} cm^{-3}) involved alternative B-site metals. Two studies did not specify which defect density was used, only mentioning the study of defects at device interfaces. The remaining 20 studies adopted N_t values equal to or above 10^{15} cm^{-3}, leading to more realistic and reliable results.

Among the strategies discussed in this work, composition engineering emerged as one of the most promising approaches to improve the performance of lead-free PSCs. This method enables the optimization of band alignment at the perovskite/ETL and perovskite/HTL interfaces, facilitating charge extraction and reducing recombination losses. Furthermore, advanced research on HTL-free and homojunction PSCs may offer a viable path toward enhancing the stability and cost-effectiveness of these devices.

Concerning composition engineering, relatively few works have applied this approach to perovskites with alternative metals, while tin-based PSCs have more frequently used this method. In these latter cases, there is a tendency to adopt idealized N_t values. In contrast, studies using tin-based PSCs generally use more realistic N_t values, typically within the range of 10^{15}–10^{17} cm^{-3}, resulting in efficiencies below 20%. While

these results appear more consistent with experimental observations, they are still noticeably higher than the best-performing lead-free PSCs reported to date, which reach around 14%.

It is important to emphasize that perovskites incorporating alternative B-site metals, other than tin, have received little experimental attention. The lack of practical studies to support the simulation findings limits a realistic assessment of their photovoltaic potential. It may partly explain the frequent use of idealized parameters in such simulations.

Therefore, the relevance of simulation studies for the development of Pb-free PSCs is emphasized, provided that realistic parameters are used. Advances in such simulations, combined with experimental research, represent a significant step forward in the pursuit of more sustainable and efficient solar cells.

Author contributions

Vívian Araújo and Leandro dos Santos conducted the literature search. Vívian Araújo analyzed the studies, wrote the initial draft, and performed the final revisions and editing. Leandro dos Santos contributed to the writing and critically revised the manuscript. Ana Nogueira and Juliana Tristão reviewed the final version and supervision.

Conflicts of interest

There are no conflicts to declare.

Data availability

As this article is a critical review, no new experimental data were generated or analyzed.

Acknowledgements

We would like to thank CAPES and FAPEMIG for supporting our research project. We also wish to thank Professor Marc Burgelman and the Electronics and Information Systems (ELIS), University of Gent of Belgium, for providing free access to the SCAPS 1D simulation tool.

References

1 E. Raphael, M. N. Silva, R. Szostak, M. A. Schiavon and A. F. Nogueira, *Quim. Nova*, 2018, **41**, 61–74.
2 K. P. Goetz, A. D. Taylor, Y. J. Hofstetter and Y. Vaynzof, *ACS Appl. Mater. Interfaces*, 2020, **13**, 1–17.
3 V. H. Araújo, G. M. Fernandes, G. C. Costa, L. J. Santos and J. C. Tristão, *Rev. Virtual Quim.*, 2022, **14**, 427–442.
4 F. Hao, C. C. Stoumpos, D. H. Cao, R. P. Chang and M. G. Kanatzidis, *Nat. Photonics*, 2014, **8**, 489–494.
5 X. Jiang, H. Li, Q. Zhou, Q. Wei, M. Wei, L. Jiang, Z. Wang, Z. Peng, F. Wang, Z. Zang, *et al.*, *J. Am. Chem. Soc.*, 2021, **143**, 10970–10976.
6 M. H. Kumar, S. Dharani, W. L. Leong, P. P. Boix, R. R. Prabhakar, T. Baikie, C. Shi, H. Ding, R. Ramesh, M. Asta, *et al.*, *Adv. Mater.*, 2014, **26**, 7122–7127.
7 F. Hao, C. C. Stoumpos, P. Guo, N. Zhou, T. J. Marks, R. P. Chang and M. G. Kanatzidis, *J. Am. Chem. Soc.*, 2015, **137**, 11445–11452.
8 S. J. Lee, S. S. Shin, Y. C. Kim, D. Kim, T. K. Ahn, J. H. Noh, J. Seo and S. I. Seok, *J. Am. Chem. Soc.*, 2016, **138**, 3974–3977.
9 W. Liao, D. Zhao, Y. Yu, C. R. Grice, C. Wang, A. J. Cimaroli, P. Schulz, W. Meng, K. Zhu and R.-G. Xiong, *Adv. Mater.*, 2016, **28**, 9333–9340.
10 M. A. Kamarudin, D. Hirotani, Z. Wang, K. Hamada, K. Nishimura, Q. Shen, T. Toyoda, S. Iikubo, T. Minemoto, K. Yoshino, *et al.*, *J. Phys. Chem. Lett.*, 2019, **10**, 5277–5283.
11 K. Nishimura, M. A. Kamarudin, D. Hirotani, K. Hamada, Q. Shen, S. Iikubo, T. Minemoto, K. Yoshino and S. Hayase, *Nano Energy*, 2020, **74**, 104858.
12 K. D. Jayan and V. Sebastian, *Sol. Energy*, 2021, **217**, 40–48.
13 M. S. Salem, A. Shaker, A. Zekry, M. Abouelatta, A. Alanazi, M. T. Alshammari and C. Gontand, *Energies*, 2021, **14**, 5741.
14 M. Kumar, A. Raj, A. Kumar and A. Anshul, *Opt. Mater.*, 2020, **108**, 110213.
15 I. Chabri, Y. Benhouria, A. Oubelkacem, A. Kaiba, I. Essaoudi and A. Ainane, *J. Electron. Mater.*, 2023, **52**, 2722–2736.
16 H.-J. Du, W.-C. Wang and J.-Z. Zhu, *Chin. Phys. B*, 2016, **25**, 108802.
17 D. Jalalian, A. Ghadimi and A. Kiani, *Eur. Phys. J.:Appl. Phys.*, 2019, **87**, 10101.
18 A. Niemegeers and M. Burgelman, *Conference Record of the Twenty Fifth IEEE Photovoltaic Specialists Conference-1996*, 1996, pp. 901–904.
19 A. C. Nkele, I. S. Ike, S. Ezugwu, M. Maaza and F. I. Ezema, *Int. J. Energy Res.*, 2021, **45**, 1496–1516.
20 Y. Liu, M. Liu, H. Yang, Z. Yi, H. Zhang, C. Tang, J. Deng, J. Wang and B. Li, *Phys. Lett. A*, 2025, 130653.
21 W. Wang, E. Quan, M. Xie and L. Chen, *J. Comput. Electron.*, 2025, **24**, 1–10.
22 A. Saidarsan, S. Guruprasad, A. Malik, P. Basumatary and D. S. Ghosh, *Sol. Energy Mater. Sol. Cells*, 2025, **279**, 113230.
23 M. Jobayer, M. A. H. Shaikat, M. Naimur Rashid and M. R. Hasan, *Heliyon*, 2023, **9**, e16815.
24 Y. Liu, X. Tan, J. Liang, H. Han, P. Xiang and W. Yan, *Adv. Funct. Mater.*, 2023, **33**, 2214271.
25 S. Bhatti, H. U. Manzoor, B. Michel, R. S. Bonilla, R. Abrams, A. Zoha, S. Hussain and R. Ghannam, *Adv. Energy Sustainability Res.*, 2023, **4**, 2300004.
26 T. M. Khan, B. Islam, M. M. Rahaman, M. M. Shakil, M. F. Rahman and S. R. Al Ahmed, *Sol. Energy Mater. Sol. Cells*, 2025, **282**, 113388.
27 A. I. Shimul, M. Khan, A. Rayhan and A. Ghosh, *Adv. Theory Simul.*, 2025, 2500182.
28 T. M. Khan and S. R. A. Ahmed, *Adv. Theory Simul.*, 2024, **7**, 2400353.
29 E. Danladi, D. S. Dogo, S. U. Michael, F. O. Uloko and A. A. O. Salawu, *East Eur. J. Phys.*, 2021, 5–17.
30 D. Li, L. Song, Y. Chen and W. Huang, *Adv. Sci.*, 2020, **7**, 1901397.

31 S. Bhattarai, A. Mhamdi, I. Hossain, Y. Raoui, R. Pandey, J. Madan, A. Bouazizi, M. Maiti, D. Gogoi and A. Sharma, *Micro Nanostruct.*, 2022, **172**, 207450.
32 S. M. Hasnain, *Sol. Energy*, 2023, **262**, 111825.
33 C. Liu, W. Li, J. Fan and Y. Mai, *J. Energy Chem.*, 2018, **27**, 1054–1066.
34 E. Aktas, N. Rajamanickam, J. Pascual, S. Hu, M. H. Aldamasy, D. Di Girolamo, W. Li, G. Nasti, E. Martínez-Ferrero, A. Wakamiya, *et al.*, *Commun. Mater.*, 2022, **3**, 104.
35 Y. Li, H. Xie, E. L. Lim, A. Hagfeldt and D. Bi, *Adv. Energy Mater.*, 2022, **12**, 2102730.
36 S. Chatterjee and A. J. Pal, *J. Mater. Chem. A*, 2018, **6**, 3793–3823.
37 J. Prakash, A. Singh, G. Sathiyan, R. Ranjan, A. Singh, A. Garg and R. K. Gupta, *Mater. Today Energy*, 2018, **9**, 440–486.
38 A. Mahapatra, D. Prochowicz, M. M. Tavakoli, S. Trivedi, P. Kumar and P. Yadav, *J. Mater. Chem. A*, 2020, **8**, 27–54.
39 N. Gamal, S. H. Sedky, A. Shaker and M. Fedawy, *Optik*, 2021, **242**, 167306.
40 H. Sabbah, J. Arayro and R. Mezher, *Materials*, 2022, **15**, 4761.
41 H. Ferhati, F. AbdelMalek and F. Djeffal, *Sol. Energy*, 2023, **262**, 111805.
42 S. Sajid, S. Alzahmi, I. B. Salem, J. Park and I. M. Obaidat, *Nanomaterials*, 2023, **13**, 983.
43 V. H. D. Araújo, A. F. Nogueira, J. C. Tristão and L. J. Dos Santos, *RSC Adv.*, 2024, **14**, 10930–10941.
44 F. Khan, T. Alshahrani, S. K. Ali, A. M. Alanazi, A. H. Alsehli, M. M. Alsowayigh, N. E. Ahmed, *et al.*, *Mater. Sci. Eng., B*, 2024, **301**, 117209.
45 G. G. Njema and J. K. Kibet, *Int. J. Photoenergy*, 2023, **2023**, 3801813.
46 Y. H. Khattak, F. Baig, H. Toura, S. Beg and B. M. Soucase, *J. Electron. Mater.*, 2019, **48**, 5723–5733.
47 S. Abdelaziz, A. Zekry, A. Shaker and M. Abouelatta, *Opt. Mater.*, 2020, **101**, 109738.
48 A. C. Piñón Reyes, R. C. Ambrosio Lázaro, K. Monfil Leyva, J. A. Luna López, J. Flores Méndez, A. H. Heredia Jiménez, A. L. Muñoz Zurita, F. Severiano Carrillo and E. Ojeda Durán, *Micromachines*, 2021, **12**, 1508.
49 A. K. Das, R. Mandal and D. Mandal, *Opt. Quantum Electron.*, 2022, **54**, 455.
50 S. Mushtaq, S. Tahir, A. Ashfaq, R. S. Bonilla, M. Haneef, R. Saeed, W. Ahmad and N. Amin, *Sol. Energy*, 2023, **249**, 401–413.
51 M. K. Hossain, M. S. Uddin, G. I. Toki, M. K. Mohammed, R. Pandey, J. Madan, M. F. Rahman, M. R. Islam, S. Bhattarai, H. Bencherif, *et al.*, *RSC Adv.*, 2023, **13**, 23514–23537.
52 M. K. Hossain, G. I. Toki, A. Kuddus, M. H. Rubel, M. Hossain, H. Bencherif, M. F. Rahman, M. R. Islam and M. Mushtaq, *Sci. Rep.*, 2023, **13**, 2521.
53 T. AlZoubi, W. J. Kadhem, M. Al Gharram, G. Makhadmeh, M. A. Abdelfattah, A. Abuelsamen, A. M. Al-Diabat, O. Abu Noqta, B. Lazarevic, S. H. Zyoud, *et al.*, *Nanomaterials*, 2024, **14**, 1062.
54 N. Singh, A. Agarwal and M. Agarwal, *J. Phys. Chem. Solids*, 2024, **186**, 111834.
55 H. Zhang, X. Ji, H. Yao, Q. Fan, B. Yu and J. Li, *Sol. Energy*, 2022, **233**, 421–434.
56 M. K. Assadi, S. Bakhoda, R. Saidur and H. Hanaei, *Renewable Sustainable Energy Rev.*, 2018, **81**, 2812–2822.
57 T. Du, W. Xu, S. Xu, S. R. Ratnasingham, C.-T. Lin, J. Kim, J. Briscoe, M. A. McLachlan and J. R. Durrant, *J. Mater. Chem. C*, 2020, **8**, 12648–12655.
58 U. Krishnan, M. Kaur, M. Kumar and A. Kumar, *J. Photonics Energy*, 2019, **9**, 021001.
59 L. Meng, J. You, T.-F. Guo and Y. Yang, *Acc. Chem. Res.*, 2016, **49**, 155–165.
60 M. Lazemi, S. Asgharizadeh and S. Bellucci, *Phys. Chem. Chem. Phys.*, 2018, **20**, 25683–25692.
61 A. Sunny, S. Rahman, M. Khatun, S. R. A. Ahmed, *et al.*, *AIP Adv.*, 2021, **11**, 065102.
62 A. Singh, U. K. Verma, S. Ameen, *et al.*, *J. Phys. Chem. Solids*, 2024, **186**, 111817.
63 M. Shamna, K. Nithya and K. Sudheer, *Mater. Today: Proc.*, 2020, **33**, 1246–1251.
64 S. Yasin, T. Al Zoubi and M. Moustafa, *Optik*, 2021, **229**, 166258.
65 E. Danladi, A. O. Salawu, M. O. Abdulmalik, E. D. Onoja, E. E. Onwoke and D. S. Adepehin, *Phys. Access*, 2022, **2**, 1–11.
66 M. R. Filip and F. Giustino, *J. Phys. Chem. C*, 2016, **120**, 166–173.
67 C. Wu, Q. Zhang, G. Liu, Z. Zhang, D. Wang, B. Qu, Z. Chen and L. Xiao, *Adv. Energy Mater.*, 2020, **10**, 1902496.
68 Q. Chen, Y. Shen, R. Cai, Z. Zhao and G. Dong, *Nanoscale*, 2025, **17**, 4892–4905.
69 K. Chakraborty, M. G. Choudhury and S. Paul, *Sol. Energy*, 2019, **194**, 886–892.
70 S. S. Hussain, S. Riaz, G. A. Nowsherwan, K. Jahangir, A. Raza, M. J. Iqbal, I. Sadiq, S. M. Hussain and S. Naseem, *J. Renewable Energy*, 2021, **2021**, 6668687.
71 A. Ashfaq, S. Tahir, S. Mushtaq, R. S. Alqurashi, M. Haneef, N. Almousa, U. ur Rehman and R. S. Bonilla, *Mater. Today Commun.*, 2023, **35**, 106016.
72 R. Kundara and S. Baghel, *Opt. Quantum Electron.*, 2023, **55**, 968.
73 I. Hasan, T. M. Khan, B. Islam, M. F. Rahman and S. R. Al Ahmed, *Mater. Sci. Eng., B*, 2024, **310**, 117740.
74 X. Zhang, H. Zhou, C. Hu, Y. Zhao, X. Ma, J. Wu, Y. Qi, W. Fang, S. Jia and J. Yu, *Sol. Energy Mater. Sol. Cells*, 2023, **260**, 112487.
75 M. Noman, A. H. H. Khan and S. T. Jan, *Sci. Rep.*, 2024, **14**, 5449.
76 M. Z. Abbasi, A. U. Rehman, M. Sheraz, W. U. K. Tareen, M. Kaleem, S. T. Jan, H. Ali and T. C. Chuah, *Results Eng.*, 2025, 105043.
77 N. Lakhdar and A. Hima, *Opt. Mater.*, 2020, **99**, 109517.
78 S. Ahmed, F. Jannat, M. A. K. Khan and M. A. Alim, *Optik*, 2021, **225**, 165765.
79 Y. He, L. Xu, C. Yang, X. Guo and S. Li, *Nanomaterials*, 2021, **11**, 2321.

80 D. Jayan K and V. Sebastian, *Adv. Theory Simul.*, 2021, **4**, 2100027.
81 K. Ahmad, W. Raza, R. A. Khan, A. Alsalme and H. Kim, *Nanomaterials*, 2022, **12**, 3407.
82 I. Chabri, A. Oubelkacem and Y. Benhouria, Numerical development of lead-free Cs_2TiI_6 based perovskite solar cell via SCAPS-1D, *E3S Web of Conferences*, 2022, vol. 336, pp. 1–8.
83 G. Pindolia, S. M. Shinde and P. K. Jha, *Sol. Energy*, 2022, **236**, 802–821.
84 S. T. Jan and M. Noman, *Sol. Energy*, 2022, **237**, 29–43.
85 W. Ahmad, M. Noman, S. Tariq Jan and A. D. Khan, *R. Soc. Open Sci.*, 2023, **10**, 221127.
86 M. K. Hossain, G. Ishraque Toki, D. Samajdar, M. Rubel, M. Mushtaq, M. R. Islam, M. F. Rahman, S. Bhattarai, H. Bencherif, M. K. Mohammed, *et al.*, *Energy Fuels*, 2023, **37**, 7380–7400.
87 B. Saparov, F. Hong, J.-P. Sun, H.-S. Duan, W. Meng, S. Cameron, I. G. Hill, Y. Yan and D. B. Mitzi, *Chem. Mater.*, 2015, **27**, 5622–5632.
88 K. M. Boopathi, P. Karuppuswamy, A. Singh, C. Hanmandlu, L. Lin, S. A. Abbas, C. C. Chang, P. C. Wang, G. Li and C. W. Chu, *J. Mater. Chem. A*, 2017, **5**, 20843–20850.
89 M. Mehrabian, M. Taleb-Abbasi and O. Akhavan, *Environ. Sci. Pollut. Res.*, 2023, **30**, 118754–118763.
90 U. U. Rehman, K. U. Sahar, E. Hussain and C.-M. Wang, *Sol. Energy*, 2024, **277**, 112752.
91 K. I. F. Utsho, S. Mostafa, M. Tarekuzzaman, M. S. Al-Saleem, N. I. Nahid, J. Y. Al-Humaidi, M. Rasheduzzaman, M. M. Rahman and M. Z. Hasan, *RSC Adv.*, 2025, **15**, 2184–2204.
92 R. Kundara and S. Baghel, *Sol. Energy*, 2025, **287**, 113253.
93 A. I. Shimul, A. Ghosh, M. F. Ahmed, A. S. Mugdho, Z. Hasan, N. S. Awwad and H. A. Ibrahium, *Langmuir*, 2025, **41**, 13655–13674.
94 A. Ijam, *Results Eng.*, 2025, 105180.
95 M. H. Miah, M. B. Rahman, F. Khatun, M. U. Khandaker, S. F. W. M. Hatta, N. B. Soin and M. A. Islam, *Optik*, 2023, **281**, 170819.
96 N. A. Mahammedi, A. Benameur, H. Gueffaf, B. Merabet, O. M. Ozkendir and S.-I. Sato, *Optik*, 2024, **302**, 171659.
97 M. Rahaman, M. Hasan, R. M. Moinuddin and M. N. Islam, *AIP Adv.*, 2024, **14**, 095019.
98 B. K. Ravidas, A. R. Kumar, A. Praveen, S. K. Agnihotri, S. Bhattarai, R. Pandey, J. Madan, S. Singh, M. K. Hossain, M. K. Roy, *et al.*, *J. Phys. Chem. Solids*, 2025, **196**, 112325.
99 S. Z. Haider, H. Anwar, Y. Jamil and M. Shahid, *J. Phys. Chem. Solids*, 2020, **136**, 109147.